



### **Science Arts & Métiers (SAM)**

is an open access repository that collects the work of Arts et Métiers Institute of Technology researchers and makes it freely available over the web where possible.

This is an author-deposited version published in: <https://sam.ensam.eu>  
Handle ID: <http://hdl.handle.net/10985/9880>

#### **To cite this version :**

Fabrice DETREZ, Olivier CASTELNAU, Patrick CORDIER, Sébastien MERKEL, Paul RATERRON - Effective viscoplastic behavior of polycrystalline aggregates lacking four independent slip systems inferred from homogenization methods; application to olivine - Journal of the Mechanics and Physics of Solids - Vol. 83, p.199-220 - 2015

Any correspondence concerning this service should be sent to the repository

Administrator : [scienceouverte@ensam.eu](mailto:scienceouverte@ensam.eu)



# Effective viscoplastic behavior of polycrystalline aggregates lacking four independent slip systems inferred from homogenization methods; application to olivine

F. Detrez<sup>a,c,\*</sup>, O. Castelnau<sup>a</sup>, P. Cordier<sup>b</sup>, S. Merkel<sup>b</sup>, P. Raterron<sup>b</sup>

<sup>a</sup> Arts et Métiers ParisTech, PIMM - UMR CNRS 8006, 151 Bd de l'Hôpital, 75013 Paris, France

<sup>b</sup> Univ Lille Nord de France, Unité Matériaux et Transformations, USTLille - CNRS UMR 8207, Cité Scientifique, Batiment C6, 59655 Villeneuve d'Ascq, France

<sup>c</sup> Université Paris-Est, Laboratoire Modélisation et Simulation Multi Echelle MSME UMR 8208 CNRS, 5 bd Descartes, F-77545 Marne-la-Vallée, France

---

## A B S T R A C T

Polycrystalline aggregates lacking four independent systems for the glide of dislocations can deform in a purely viscoplastic regime only if additional deformation mechanisms (such as grain boundary sliding and diffusion) are activated. We introduce an implementation of the self-consistent scheme in which this additional physical mechanism, considered as a stress relaxation mechanism, is represented by a nonlinear isotropic viscoplastic potential. Several nonlinear extensions of the self-consistent scheme, including the second-order method of Ponte-Castañeda, are used to provide an estimate of the effective viscoplastic behavior of such polycrystals. The implementation of the method includes an approximation of the isotropic potential to ensure convergence of the attractive fixed-point numerical algorithm. The method is then applied to olivine polycrystals, the main constituent of the Earth's upper mantle. Due to the extreme local anisotropy of the local constitutive behavior and the subsequent intraphase stress and strain-rate field heterogeneities, the second-order method is the only extension providing qualitative and quantitative accurate results. The effective viscosity is strongly dependent on the strength of the relaxation mechanism. For olivine, a linear viscous relaxation (e.g. diffusion) could be relevant; in that case, the polycrystal stress sensitivity is reduced compared to that of dislocation glide, and the most active slip system is not necessarily the one with the smallest reference stress due to stress concentrations. This study reveals the significant importance of the strength and stress sensitivity of the additional relaxation mechanism for the rheology and lattice preferred orientation in such highly anisotropic polycrystalline aggregates.

---

### Keywords:

Viscoplasticity  
Polycrystal  
Non-linear homogenization  
Anisotropy  
Self-consistent scheme  
Olivine  
Earth mantle

---

\* Corresponding author at: Université Paris-Est, Laboratoire Modélisation et Simulation Multi Echelle MSME UMR 8208 CNRS, 5 bd Descartes, F-77545 Marne-la-Vallée, France.

E-mail addresses: [fabrice.detrez@univ-paris-est.fr](mailto:fabrice.detrez@univ-paris-est.fr) (F. Detrez), [olivier.castelnau@ensam.fr](mailto:olivier.castelnau@ensam.fr) (O. Castelnau), [Patrick.Cordier@univ-lille1.fr](mailto:Patrick.Cordier@univ-lille1.fr) (P. Cordier), [sebastien.merkel@univ-lille1.fr](mailto:sebastien.merkel@univ-lille1.fr) (S. Merkel), [Paul.Raterron@univ-lille1.fr](mailto:Paul.Raterron@univ-lille1.fr) (P. Raterron).

**Table 1**  
List of acronyms.

FFT	Fast Fourier transform
LPO	Lattice preferred orientation
SC	Self-consistent model
SEC	Secant estimate
TGT	Tangent estimate
AFF	Affine estimate
VAR	Variational estimate
SO	Second-order estimate
NPLCP	N-phase linear comparison polycrystal

## 1. Introduction

Physically based scale transition models are essential to establish the relation between the microstructure of polycrystalline aggregates and their effective viscoplastic properties. The accuracy of predictions is a key parameter to understand and model texture evolutions and the induced effective anisotropy. On the one hand, full-field approaches based on crystal plasticity have been proposed to compute the response of specific microstructures, using the Finite Element Method (see, e.g. [Sarma and Dawson, 1996](#); [Bhattacharya et al., 2001](#); [Kanit et al., 2003](#)) or Fast Fourier Transforms (FFT; acronyms used in this paper are listed in [Table 1](#)) (see, e.g. [Moulinec and Suquet, 1998](#); [Lebensohn, 2001](#)). Despite the development of novel and very efficient methods such as FFT, the size of simulated representative volume is limited, and computations are CPU demanding. On the other hand, mean-field approaches such as those based on the self-consistent (SC) scheme, rely on a statistical description of the microstructure and are very powerful for the prediction of the effective behavior and the development of Lattice Preferred Orientation (LPO) at large overall strain. For nonlinear behavior, the main drawback is the necessary linearization of the local constitutive behavior that can critically affect the results consistency (see [Ponte Castañeda and Suquet, 1998](#), for a review).

In this work, we will focus on the effective viscoplastic behavior of polycrystals lacking four independent slip systems. The vast majority of minerals constituting the Earth's mantle, such as olivine and pyroxenes, belongs to this class of materials ([Karato, 2007](#)). Similarly, many synthesized materials, such as semi-crystalline polymers (see, e.g. [Bowden and Young, 1974](#); [Argon, 1997](#); [Seguela, 2007](#)), do not exhibit four independent slip systems. It is worth noting that *five* independent slip systems are necessary to accommodate any arbitrary plastic strain at the local (i.e. grain) scale – this is the so-called von Mises criterion. However, SC estimations ([Hutchinson, 1977](#); [Nebozhyn et al., 2000](#)) but also full-field computations ([Castelnau et al., 2008a](#); [Lebensohn et al., 2011](#)) have shown that *four* independent systems are sufficient to ensure the polycrystal to deform as a whole, i.e. to guarantee a finite flow stress for any prescribed overall strain-rate.

The kinematic constraints induced by the lack of four independent slip systems lead to an indeterminacy of part of the deviatoric stress tensor. Only few attempts in the literature tried to address this issue. [Parks and Ahzi \(1990\)](#) proposed an ad hoc formulation, using Lagrange multipliers to determine unknown stress components, allowing the polycrystal to undergo viscoplastic strain with less than four independent slip systems. In the geophysical community, the purely kinematic model proposed by [Ribe and Yu \(1991\)](#), and extended by [Kaminski and Ribe \(2001\)](#) to include recrystallization effects, is widely spread and used; this relatively simple and intuitive formulation, which does not permit an estimation of the effective flow stress, also allows olivine polycrystals to deform with less than four independent slip systems, in qualitative contradiction with full-field results. Finally, a number of papers, e.g. [Wenk et al. \(1991\)](#), [Tommasi et al. \(1999, 2000\)](#), and [Blackman et al. \(2002\)](#) have applied the tangent (TGT) extension of the SC scheme ([Lebensohn and Tomé, 1993](#)) to olivine polycrystals; for purely numerical purpose, these authors introduced an artificial additional slip system with a large resistance to slip. It turns out that the TGT model incorrectly predicts a finite effective flow stress with only three independent slip systems ([Castelnau et al., 2008a,b, 2010](#)), a limitation that also affects microstructure evolutions at large strain ([Castelnau et al., 2009](#)).

Within the SC scheme, initially proposed for linear (e.g. thermo-elastic) polycrystals, all grains exhibiting the same crystal orientation are treated as a single (mechanical) phase. The SC scheme describes the statistical interaction between each phase and the surrounding polycrystal using the analytical solution of [Eshelby \(1957\)](#) to account for the interaction between an ellipsoidal inhomogeneity within a homogeneous linear matrix. The behavior of the surrounding polycrystal can then be obtained using the consistency conditions. Note that, at large strain, microstructure evolutions predicted by the SC scheme still suffer inconsistency due to an incomplete knowledge of the intragranular strain field, as illustrated in [Castelnau et al. \(2006\)](#) for the case of strain-hardening.

For nonlinear polycrystals, a linearization of the local constitutive behavior is necessary, leading to the definition of a N-Phase Linear Comparison Polycrystal (NPLCP). The standard thermo-elastic SC solution can then be applied to the NPLCP, from which the behavior of the original nonlinear polycrystal can be derived. This linearization step is not trivial, this is why several extensions of the SC scheme have been proposed in the literature, e.g. the secant (SEC)

(Hill, 1965; Hutchinson, 1976), tangent (TGT) (Molinari et al., 1987; Lebensohn and Tomé, 1993), or affine (AFF) (Masson et al., 2000) methods. These three methods do not account for the intraphase field heterogeneities for the definition of the NPLCP, and are thus limited in accuracy for moderate local anisotropy and nonlinearity. In the TGT extension, often denoted as the “VPSC model” in the literature, the thermo-elastic nature of the NPLCP has not been fully recognized; therefore the model unrealistically converges towards the uniform stress bound (Static bound) at large stress sensitivities, as detailed in Masson et al. (2000); this limitation has been corrected by the AFF extension.

More accurate estimations can be obtained with the variational procedure (VAR) (Ponte Castañeda, 1991; de Botton and Ponte Castañeda, 1995) and the second-order (SO) estimate (Ponte Castañeda, 2002; Liu and Ponte Castañeda, 2004). These two methods are accurate up to the second order Taylor expansion of the mechanical contrast, and are thus denoted as ‘second-order’ methods. The improved accuracy results from the additional use of the second order moment of the mechanical fields, which depends on the intraphase field fluctuations, to define the NPLCP. Both extensions exhibit very interesting features, such as compliance with rigorous upper bounds for the effective potential, which are generally violated by other homogenization procedures (Gilormini et al., 1995).

At present, scale transition models providing an accurate estimation of the viscoplastic behavior of polycrystals lacking four independent slip systems are still lacking. Indeed, current solutions involve either inappropriate homogenization schemes or use of artificial additional slip systems. The aim of the present work is to improve the nonlinear extensions of the SC scheme for polycrystals lacking four independent slip systems by introducing an isotropic stress relaxation mechanism. In the present work, the additional mechanism is represented by a nonlinear and isotropic viscoplastic potential in the local constitutive relation. The physical meaning of such a choice will be discussed in Section 4 for the case of olivine.

This new scheme is then applied to the case of (Mg,Fe)<sub>2</sub>SiO<sub>4</sub> olivine, the main mineral of the Earth’s upper mantle, in order to test the effect of the flow stress and stress sensitivity of this additional isotropic stress relaxation mechanism on the overall behavior of the polycrystal. In particular, we will show the importance of the stress sensitivity of the additional mechanism on the overall stress sensitivity of the polycrystal.

This paper is organized as follows. First, Section 2 describes the constitutive model used at the grain scale and the linearization extensions of the SC scheme. Section 3 is devoted to the algorithm used to solve the self-consistent equations and to compute field statistics. Section 4 presents an application to the case of olivine.

Notations are based on the following conventions. Scalars are in italics ( $a, A, \alpha$ ), vectors are underlined bold-face ( $\underline{\mathbf{a}}, \underline{\mathbf{A}}, \underline{\alpha}$ ), second-order tensors are bold-face and underlined once by a tilde ( $\underline{\underline{\mathbf{a}}}, \underline{\underline{\mathbf{A}}}, \underline{\underline{\alpha}}$ ), and fourth-order tensors are bold-face and underlined twice ( $\underline{\underline{\underline{\mathbf{a}}}}, \underline{\underline{\underline{\mathbf{A}}}}, \underline{\underline{\underline{\alpha}}}$ ). Tensor (dyadic) products are indicated by ‘ $\otimes$ ’, twice contracted tensor scalar products by ‘ $\cdot$ ’ ( $\underline{\underline{\mathbf{A}}} : \underline{\underline{\mathbf{B}}} = A_{ij}B_{ij}$ ), and four times contracted product by ‘ $\llbracket$ ’ ( $\underline{\underline{\underline{\mathbf{A}}}} :: \underline{\underline{\underline{\mathbf{B}}}} = A_{ijkl}B_{ijkl}$ ). Superscripts  $\cdot^T$  and  $\cdot^{-1}$  denote transpose and inverse, respectively. The expression  $\partial_{\underline{\mathbf{a}}}\phi$  corresponds to the differentiation of  $\phi$  with respect to  $\underline{\mathbf{a}}$ .

## 2. Model

### 2.1. Local behavior

The local behavior is assumed to be incompressible, therefore the Eulerian strain-rate tensor  $\underline{\underline{\boldsymbol{\xi}}}$  is deviatoric. Incompressibility also involves that the Eulerian strain-rate exclusively depends on the deviatoric part of stress tensor; the Cauchy stress will be considered as deviatoric and denoted  $\underline{\underline{\boldsymbol{\sigma}}}$ . For a given stress  $\underline{\underline{\boldsymbol{\sigma}}}$ , the local constitutive response is defined by

$$\underline{\underline{\boldsymbol{\xi}}} = \partial_{\underline{\underline{\boldsymbol{\sigma}}}} u^{(r)}(\underline{\mathbf{x}}, \underline{\underline{\boldsymbol{\sigma}}}) \quad (1)$$

where  $u^{(r)}$  is the stress potential for the single crystals at position  $\underline{\mathbf{x}}$  with lattice orientation  $\underline{\underline{\mathbf{Q}}}^{(r)}$  expressed with respect to a given external reference frame. Each single crystal stress potential  $u^{(r)}$  is decomposed into several components  $\phi_{(k)}^{(r)}$  ( $k = 1, \dots, K$ ) describing the response of each of the  $K$  slip systems, and another term  $\phi_{(0)}^{(r)}$  which describes the response of the incompressible isotropic relaxation mechanism:

$$u^{(r)}(\underline{\underline{\boldsymbol{\sigma}}}) = \phi_{(0)}^{(r)}(\sigma_e) + \sum_{k=1}^K \phi_{(k)}^{(r)}(\tau_{(k)}^{(r)}) \quad (2)$$

The convex function  $\phi_{(0)}^{(r)}(\sigma_e)$  depends on the von Mises equivalent stress  $\sigma_e$ , while  $\phi_{(k)}^{(r)}(\tau_{(k)}^{(r)})$  depends on the resolved shear stresses  $\tau_{(k)}^{(r)}$  on system  $(k)$ , defined by

$$\sigma_e = \sqrt{\frac{3}{2} \underline{\underline{\boldsymbol{\sigma}}} : \underline{\underline{\boldsymbol{\sigma}}}}, \quad \tau_{(k)}^{(r)} = \underline{\underline{\boldsymbol{\mu}}}_{(k)}^{(r)} : \underline{\underline{\boldsymbol{\sigma}}} \quad (3)$$

where  $\underline{\underline{\boldsymbol{\mu}}}_{(k)}^{(r)} = \frac{1}{2} \left( \underline{\underline{\mathbf{n}}}_{(k)}^{(r)} \otimes \underline{\underline{\mathbf{m}}}_{(k)}^{(r)} + \underline{\underline{\mathbf{m}}}_{(k)}^{(r)} \otimes \underline{\underline{\mathbf{n}}}_{(k)}^{(r)} \right)$  are the Schmid tensors expressing the orientation of the slip system with respect to the reference frame. Here,  $\underline{\underline{\mathbf{n}}}_{(k)}^{(r)}$  and  $\underline{\underline{\mathbf{m}}}_{(k)}^{(r)}$  denote the unit vectors normal to the slip plane and along the slip direction of the system  $(k)$  in phase  $(r)$ , respectively, for a crystal with orientation  $\underline{\underline{\mathbf{Q}}}^{(r)}$ . We consider slip potentials and relaxation potential

given by a power-law

$$\phi_{(k)}^{(r)}(\tau) = \gamma_0 \frac{(\tau_0)_{(k)}}{n_{(k)} + 1} \left( \frac{|\tau_{(k)}^{(r)}|}{(\tau_0)_{(k)}} \right)^{n_{(k)}+1} \quad (4)$$

$$\phi_{(0)}^{(r)}(\sigma_e) = \varepsilon_0 \frac{\sigma_0}{n_{(0)} + 1} \left( \frac{\sigma_e^{(r)}}{\sigma_0} \right)^{n_{(0)}+1} \quad (5)$$

where  $n_{(k)} \geq 1$  and  $(\tau_0)_{(k)} > 0$  are the stress sensitivity and reference flow stress for the slip system  $(k)$ , respectively, and  $n_{(0)} \geq 1$  and  $\sigma_0 > 0$  are the stress sensitivity and reference flow stress for the isotropic relaxation mechanism.

## 2.2. Basic features of mean-field theories

Mean-field theories are limited to a statistical description of the microstructure. All grains are sorted in a set of  $N$  phases, each with a given lattice orientation characterized by the rotation tensor  $\mathbf{Q}^{(r)}$  ( $r = 1, \dots, N$ ). Grain shape are assumed to be ellipsoidal on average with identical aspect ratios for all phases (see Willis, 1977, for the mathematical description of microstructure). We denote  $\Omega$  the region occupied by the polycrystal, and  $\Omega^{(r)}$  the subregions occupied by the mechanical phase  $(r)$ . The characteristic functions  $\chi^{(r)}(\mathbf{x})$  describing the geometry of  $\Omega^{(r)}$  are equal to 1 if the position vector  $\mathbf{x}$  lies in  $\Omega^{(r)}$ , and zero otherwise. Volume averages over  $\Omega$  are denoted by  $\langle \cdot \rangle$ , and volume average over  $\Omega^{(r)}$  by  $\langle \cdot \rangle^{(r)}$ . Volume fraction  $c^{(r)} = \langle \chi^{(r)} \rangle$  of phase  $(r)$  also characterizes the crystallographic texture of the polycrystal.

The effective viscoplastic response of the polycrystal may be written in the form (see e.g. Ponte Castañeda and Suquet, 1998, for a comprehensive review)

$$\tilde{\boldsymbol{\varepsilon}} = \partial_{\boldsymbol{\sigma}} \tilde{U}, \quad \tilde{U}(\tilde{\boldsymbol{\sigma}}) = \text{stat}_{\boldsymbol{\sigma} \in \mathcal{S}(\tilde{\boldsymbol{\sigma}})} \langle u(\mathbf{x}, \boldsymbol{\sigma}) \rangle = \text{stat}_{\boldsymbol{\sigma} \in \mathcal{S}(\tilde{\boldsymbol{\sigma}})} \sum_{r=1}^N c^{(r)} \langle u^{(r)}(\boldsymbol{\sigma}) \rangle^{(r)} \quad (6)$$

where  $\tilde{U}$  is the effective stress potential for the polycrystal, and the set of statically admissible stresses is assigned by  $\mathcal{S}(\tilde{\boldsymbol{\sigma}}) = \{\boldsymbol{\sigma}, \text{div } \boldsymbol{\sigma} = \mathbf{0} \text{ in } \Omega, \langle \boldsymbol{\sigma} \rangle = \tilde{\boldsymbol{\sigma}}\}$ . In relation (6),  $\tilde{\boldsymbol{\varepsilon}} = \langle \boldsymbol{\varepsilon} \rangle$  and  $\tilde{\boldsymbol{\sigma}} = \langle \boldsymbol{\sigma} \rangle$  are the average strain-rate and the average stress, respectively.

Let us assume the existence of a NPLCP which has the same microstructure as the nonlinear polycrystal of interest. This NPLCP, which local behavior is of a linear thermo-elastic type and to which the linear SC scheme applies, is an approximation of the actual nonlinear polycrystal. This assumption leads to the definition of a linear local stress potential  $u_L^{(r)}(\boldsymbol{\sigma})$  for phase  $(r)$

$$u_L(\mathbf{x}, \boldsymbol{\sigma}) = \sum_{r=1}^N \chi^{(r)}(\mathbf{x}) u_L^{(r)}(\boldsymbol{\sigma}), \quad u_L^{(r)}(\boldsymbol{\sigma}) = \frac{1}{2} \boldsymbol{\sigma} : \tilde{\mathbf{M}}^{(r)} : \boldsymbol{\sigma} + \boldsymbol{\varepsilon}^{(r)} : \boldsymbol{\sigma} \quad (7)$$

where  $\tilde{\mathbf{M}}^{(r)}$  and  $\boldsymbol{\varepsilon}^{(r)}$  are the viscoplastic compliance and the eigen-strain-rate of phase  $(r)$ , respectively. The effective potential  $\tilde{U}_L$  of the NPLCP may be written in the form (Laws, 1973; Willis, 1981)

$$\tilde{U}_L(\tilde{\boldsymbol{\sigma}}) = \frac{1}{2} \tilde{\boldsymbol{\sigma}} : \tilde{\mathbf{M}} : \tilde{\boldsymbol{\sigma}} + \tilde{\boldsymbol{\varepsilon}} : \tilde{\boldsymbol{\sigma}} + \tilde{g} \quad (8)$$

where  $\tilde{\mathbf{M}}$ ,  $\tilde{\boldsymbol{\varepsilon}}$  and  $\tilde{g}$  are the effective compliance, eigen-strain-rate and energy under zero applied stress, defined by

$$\tilde{\mathbf{M}} = \sum_{r=1}^N c^{(r)} \tilde{\mathbf{M}}^{(r)} : \tilde{\mathbf{B}}^{(r)}, \quad \tilde{\boldsymbol{\varepsilon}} = \sum_{r=1}^N c^{(r)} \boldsymbol{\varepsilon}^{(r)} : \tilde{\mathbf{B}}^{(r)}, \quad \tilde{g} = \sum_{r=1}^N c^{(r)} \boldsymbol{\varepsilon}^{(r)} : \tilde{\mathbf{b}}^{(r)}. \quad (9)$$

Here,  $\tilde{\mathbf{B}}^{(r)}$  and  $\tilde{\mathbf{b}}^{(r)}$  are the phase average concentration tensors depending on the microstructure, and the mean stress in phase  $(r)$  of the NPLCP reads (Ponte Castañeda and Suquet, 1998)

$$\tilde{\boldsymbol{\sigma}}_L^{(r)} = \langle \boldsymbol{\sigma} \rangle_L^{(r)} = \tilde{\mathbf{B}}^{(r)} : \tilde{\boldsymbol{\sigma}} + \tilde{\mathbf{b}}^{(r)}. \quad (10)$$

For the self-consistent scheme, the expressions for  $\tilde{\mathbf{B}}^{(r)}$  and  $\tilde{\mathbf{b}}^{(r)}$  in a general context of anisotropy can be found e.g. in Brenner et al. (2004) or Lebensohn et al. (2011). The field statistics in the NPLCP are obtained by differentiation of effective potential  $\tilde{U}_L$  with respect to appropriate parameters

$$\tilde{\boldsymbol{\sigma}}_L^{(r)} = \frac{1}{c^{(r)}} \partial_{\boldsymbol{\varepsilon}^{(r)}} \tilde{U}_L(\tilde{\boldsymbol{\sigma}}), \quad \langle \boldsymbol{\sigma} \otimes \boldsymbol{\sigma} \rangle_L^{(r)} = \frac{2}{c^{(r)}} \partial_{\tilde{\mathbf{M}}^{(r)}} \tilde{U}_L(\tilde{\boldsymbol{\sigma}}). \quad (11)$$

It is interesting to note that, rigorously, the stress and strain-rate distributions (and thus their moments) in the NPCPL are a priori not identical to those in the nonlinear polycrystal. For the sake of simplicity, we assume here that both match with each other

$$\underline{\underline{\boldsymbol{\sigma}}}^{(r)} \approx \underline{\underline{\boldsymbol{\sigma}}}_L^{(r)}, \quad \langle \underline{\underline{\boldsymbol{\sigma}}} \otimes \underline{\underline{\boldsymbol{\sigma}}} \rangle^{(r)} \approx \langle \underline{\underline{\boldsymbol{\sigma}}} \otimes \underline{\underline{\boldsymbol{\sigma}}} \rangle_L^{(r)}. \quad (12)$$

This is an inherent assumption of all standard homogenization schemes used here, while for Ponte Castaneda's formulation, it is the only numerically tractable solution – which has been shown in a number of papers to provide results in very good agreement with reference results from full-field methods.

The knowledge of  $\underline{\underline{\boldsymbol{\sigma}}}^{(r)}$  for all crystal orientations ( $r$ ) allows investigating of the so-called “interphase” heterogeneities, i.e. the variation of the phase average stress with respect to the crystal orientation. Deeper insight into the stress distribution can be obtained from the second moment  $\langle \underline{\underline{\boldsymbol{\sigma}}} \otimes \underline{\underline{\boldsymbol{\sigma}}} \rangle^{(r)}$ . Its expression for the SC scheme can be found in [Bobeth and Diener \(1987\)](#), [Kreher \(1990\)](#), [Brenner et al. \(2004\)](#), and [Lebensohn et al. \(2011\)](#). Note that the variance of the stress within a given crystal orientation can be estimated from the covariance tensor of stress fluctuations  $\underline{\underline{\boldsymbol{c}}}_{\underline{\underline{\boldsymbol{\sigma}}}}^{(r)}$  inside phase ( $r$ ) as

$$\underline{\underline{\boldsymbol{c}}}_{\underline{\underline{\boldsymbol{\sigma}}}}^{(r)} = \langle \underline{\underline{\boldsymbol{\sigma}}} \otimes \underline{\underline{\boldsymbol{\sigma}}} \rangle^{(r)} - \underline{\underline{\boldsymbol{\sigma}}}^{(r)} \otimes \underline{\underline{\boldsymbol{\sigma}}}^{(r)} \quad (13)$$

which is related to the width of the stress distribution within phase ( $r$ ). Similar relations can be derived for the strain-rate statistics.

### 2.3. Different possible linearizations

The difficult part of the problem consists in finding the linearization procedure leading to the optimal choice of the NPLCP. As stated earlier, the local behavior at the phase level, Eq. (7), can be linearized in different ways, and results of the homogenization scheme unfortunately depend on this choice. Within the secant (SEC) ([Hill, 1965](#); [Hutchinson, 1976](#)) and affine (AFF) ([Masson et al., 2000](#)) linearization procedures, the phase average strain-rate is *assumed* to be defined as

$$\underline{\underline{\boldsymbol{\varepsilon}}}^{(r)} = \partial_{\underline{\underline{\boldsymbol{\sigma}}}} \phi^{(r)}(\underline{\underline{\boldsymbol{\sigma}}}^{(r)}). \quad (14)$$

The SEC approximation leads to an ‘elastic-type’ linearized behavior

$$\underline{\underline{\boldsymbol{\varepsilon}}}^{(r)} = \underline{\underline{\boldsymbol{M}}}_{SEC}^{(r)} : \underline{\underline{\boldsymbol{\sigma}}}^{(r)}, \quad \underline{\underline{\boldsymbol{e}}}_{SEC}^{(r)} = \underline{\underline{\boldsymbol{0}}}, \quad (15)$$

whereas the AFF one is based on the simple and intuitive idea of a linear behavior tangent to the nonlinear one (‘thermo-elastic-type’ linearized behavior)

$$\underline{\underline{\boldsymbol{M}}}_{AFF}^{(r)} = \partial_{\underline{\underline{\boldsymbol{\sigma}}}}^2 \phi^{(r)}(\underline{\underline{\boldsymbol{\sigma}}}^{(r)}), \quad \underline{\underline{\boldsymbol{e}}}_{AFF}^{(r)} = \underline{\underline{\boldsymbol{\varepsilon}}}^{(r)} - \underline{\underline{\boldsymbol{M}}}_{AFF}^{(r)} : \underline{\underline{\boldsymbol{\sigma}}}^{(r)}. \quad (16)$$

The main limitations of these procedures are discussed in detail e.g. in [Bornert and Ponte Castañeda \(1998\)](#) and [Masson et al. \(2000\)](#). One of them is the violation of rigorous upper bounds for the effective behavior. More generally, the affine extension is known to overestimate the overall viscosity, i.e. to predict too stiff effective behaviors. This negative feature can be alleviated by means of the energy formulation originally proposed by [Ponte Castañeda \(1996\)](#) (see, e.g. [Bornert et al., 2001](#)). The SEC procedure generally provides results even stiffer than the AFF one.

In the case of the tangent (TGT) approximation ([Molinari et al., 1987](#); [Lebensohn and Tomé, 1993](#)), the moduli are, formally, the same as in the AFF case:  $\underline{\underline{\boldsymbol{M}}}_{TGT}^{(r)} = \underline{\underline{\boldsymbol{M}}}_{AFF}^{(r)}$  and  $\underline{\underline{\boldsymbol{e}}}_{TGT}^{(r)} = \underline{\underline{\boldsymbol{e}}}_{AFF}^{(r)}$ . However, instead of using these moduli, [Molinari et al. \(1987\)](#) used the associated secant compliances to estimate the effective compliance, in combination with the tangent-secant relation  $\underline{\underline{\boldsymbol{M}}}_{TGT} = n \underline{\underline{\boldsymbol{M}}}_{SEC}$  ([Hutchinson, 1976](#)). Besides the inconsistency described in [Masson et al. \(2000\)](#), this procedure is by construction limited to power-law deformation mechanisms that all exhibit the same stress sensitivity  $n$ .

An “optimal” solution has been obtained in the context of the VAR procedure of [Ponte Castañeda \(1991\)](#), which was extended to polycrystals by [de Botton and Ponte Castañeda \(1995\)](#). Here, the stress potential  $u^{(r)}$  (see Eqs. (2), (4) and (5)) can be written in term  $u^{(r)} = g^{(r)}(\underline{\underline{\boldsymbol{\sigma}}} \otimes \underline{\underline{\boldsymbol{\sigma}}})$  where  $g^{(r)}(\underline{\underline{\boldsymbol{X}}})$  is a scalar function defined in the space of symmetric fourth-order tensors  $\underline{\underline{\boldsymbol{X}}}$ . The VAR procedure which is also called “generalized secant” linearization by [Suquet \(1995\)](#), leads to ([Ponte Castañeda and Suquet, 1998](#))

$$\underline{\underline{\boldsymbol{M}}}_{VAR}^{(r)} = \partial_{\underline{\underline{\boldsymbol{X}}}} g^{(r)}(\underline{\underline{\boldsymbol{\sigma}}} \otimes \underline{\underline{\boldsymbol{\sigma}}}^{(r)}), \quad \underline{\underline{\boldsymbol{e}}}_{VAR}^{(r)} = \underline{\underline{\boldsymbol{0}}} \quad (17)$$

The detailed expressions of the compliance tensor  $\underline{\underline{\boldsymbol{M}}}_{VAR}^{(r)}$  are given in [Appendix A](#) for each linearization procedures.

### 2.4. The second-order theory

The case of the second-order method of [Ponte Castañeda \(2002\)](#) is treated in this specific section since it requires a specific numerical treatment, described below. The thermo-elastic form (7) is considered as for the local stress potential  $u_L^{(r)}(\underline{\underline{\boldsymbol{\sigma}}})$ , where the phase compliance  $\underline{\underline{\boldsymbol{M}}}_{VAR}^{(r)}$  and eigen-strain-rate  $\underline{\underline{\boldsymbol{e}}}^{(r)}$  are defined by four parameters  $\alpha_{(k)}^{(r)}$ ,  $\beta_{(i)}^{(r)}$ ,  $e_{(k)}^{(r)}$  and  $d_{(i)}^{(r)}$

$$\underline{\underline{\mathbf{M}}}^{(r)} = \sum_{k=1}^K \alpha_{(k)}^{(r)} \underline{\underline{\boldsymbol{\mu}}}_{(k)}^{(r)} \otimes \underline{\underline{\boldsymbol{\mu}}}_{(k)}^{(r)} + \sum_{i=1}^5 \beta_{(i)}^{(r)} \underline{\underline{\boldsymbol{g}}}_{(i)}^{(r)} \otimes \underline{\underline{\boldsymbol{g}}}_{(i)}^{(r)}, \quad (18)$$

$$\underline{\underline{\boldsymbol{e}}}^{(r)} = \sum_{k=1}^K e_{(k)}^{(r)} \underline{\underline{\boldsymbol{\mu}}}_{(k)}^{(r)} + \sum_{i=1}^5 d_{(i)}^{(r)} \underline{\underline{\boldsymbol{g}}}_{(i)}^{(r)}. \quad (19)$$

Here, the set of tensors  $\underline{\underline{\boldsymbol{g}}}_{(i)}^{(r)}$  forms an orthonormal basis of deviatoric symmetric tensors such as

$$\underline{\underline{\boldsymbol{g}}} = \sum_{i=1}^5 \sigma_{(i)} \underline{\underline{\boldsymbol{g}}}_{(i)}, \quad \underline{\underline{\boldsymbol{g}}}_{(i)} : \underline{\underline{\boldsymbol{g}}}_{(j)} = \delta_{ij}. \quad (20)$$

Note that the number of independent parameters  $(\alpha_{(k)}^{(r)}, \beta_{(i)}^{(r)})$  in the compliance tensors  $\underline{\underline{\mathbf{M}}}^{(r)}$  can be at most equal to the number of independent parameters  $(e_{(k)}^{(r)}, d_{(i)}^{(r)})$  in the eigen-strain-rate tensor (Idiart and Ponte Castañeda, 2005).

#### 2.4.1. Linearization of the slip potential

For the sake of clarity we will omit in the following the indices  $(\cdot)_{(k)}^{(r)}$  that relate to the slip system  $(k)$  in the phase  $(r)$ . The parameters  $\alpha$  and  $e$  are determined from a linear expansion of the difference function  $(\phi - \psi)(\tau)$  between the nonlinear potential  $\phi$  and the quadratic potential  $\psi(\tau) = \frac{1}{2}\alpha\tau^2$  introduced by Liu and Ponte Castañeda, 2004:

$$\phi(\tau) - \psi(\tau) \approx e\tau - e\hat{\tau} + \phi(\hat{\tau}) - \psi(\hat{\tau}), \quad (21)$$

where the parameters  $\hat{\tau}$  and  $e$  are determined by an extension of Legendre's transform for non-convex function:

$$e = \partial_{\tau}\phi(\hat{\tau}) - \alpha(\hat{\tau}) = \partial_{\tau}\phi(\hat{\tau}) - \alpha\hat{\tau}. \quad (22)$$

The advantage in this approximation is that the degree of freedom  $\alpha$  still exists to rewrite the nonlinear potential  $\phi$ . Indeed, the spatial average over phase  $(r)$  of the nonlinear potential  $\phi$  can be approximated by

$$\langle \phi(\tau) \rangle \approx \text{stat}_{\alpha} \left\{ \frac{1}{2}\alpha\langle \tau^2 \rangle + e(\bar{\tau} - \hat{\tau}) + \phi(\hat{\tau}) - \frac{1}{2}\alpha\hat{\tau}^2 \right\} \quad (23)$$

under the assumption that the parameters  $\alpha$ ,  $\hat{\tau}$  and  $e$  are constant within phase  $(r)$ . Here  $\bar{\tau} = \langle \tau \rangle$ , and the stationarity condition with respect  $\alpha$  leads to

$$\langle (\tau - \bar{\tau})^2 \rangle = (\hat{\tau} - \bar{\tau})^2 \quad (24)$$

which allows determining  $\hat{\tau}$ , and the conditions (22) give

$$\alpha = \frac{\partial_{\tau}\phi(\hat{\tau}) - \partial_{\tau}\phi(\bar{\tau})}{\hat{\tau} - \bar{\tau}} \quad \text{and} \quad e = \partial_{\tau}\phi(\hat{\tau}) - \alpha\hat{\tau}. \quad (25)$$

#### 2.4.2. Linearization of the isotropic relaxation potential

As above, we omit in the following the indices  $(\cdot)_{(i)}^{(r)}$  that relate to the relaxation mechanism in the phase  $(r)$  and we introduce another quadratic function

$$\psi(\sigma_{(1)}, \dots, \sigma_{(5)}) = \sum_{i=1}^5 \frac{1}{2}\beta_{(i)}\sigma_{(i)}^2 \quad (26)$$

with  $\sigma_{(i)}$  defined in (19). First, as above, the difference function  $(\phi - \psi)(\sigma_{(1)}; \sigma_{(2)}, \dots, \sigma_{(5)})$  is approximated by its expansion with respect to  $\sigma_{(1)}$

$$(\phi - \psi)(\sigma_{(1)}; \sigma_{(2)}, \dots, \sigma_{(5)}) \approx d_{(1)}\sigma_{(1)} - d_{(1)}\hat{\sigma}_{(1)} + (\phi - \psi)(\hat{\sigma}_{(1)}; \sigma_{(2)}, \dots, \sigma_{(5)}) \quad (27)$$

where the parameters  $\hat{\sigma}_{(1)}$  and  $d_{(1)}$  are given by

$$d_{(1)} = \partial_{\sigma_{(1)}}\phi(\hat{\sigma}_{(1)}; \sigma_{(2)}, \dots, \sigma_{(5)}) - \beta_{(1)}\hat{\sigma}_{(1)} = \partial_{\sigma_{(1)}}\phi(\sigma_{(1)}; \sigma_{(2)}, \dots, \sigma_{(5)}) - \beta_{(1)}\sigma_{(1)} \quad (28)$$

with  $\sigma_{(i)}$  for  $i \geq 2$  considered as variables.

Next, the difference function  $(\phi - \psi)(\hat{\sigma}_{(1)}, \sigma_{(2)}, \dots, \sigma_{(5)})$  is expanded the same way, now considering  $\sigma_{(2)}$  as a variable. After having repeated this process for all independent variables  $\sigma_{(i)}$  successively, we obtain

$$(\phi - \psi)(\underline{\underline{\boldsymbol{\sigma}}}) \approx (\phi - \psi)(\underline{\underline{\boldsymbol{\hat{\sigma}}}}) + \sum_{i=1}^5 d_{(i)}(\sigma_{(i)} - \hat{\sigma}_{(i)}) \quad (29)$$

where

$$d_{(i)} = \partial_{\sigma_{(i)}} \phi(\hat{\boldsymbol{\sigma}}) - \beta_{(i)} \hat{\sigma}_{(i)} = \partial_{\sigma_{(i)}} \phi(\boldsymbol{\sigma}) - \beta_{(i)} \sigma_{(i)}. \quad (30)$$

The differentiation of the function  $\phi$  with respect to  $\sigma_{(i)}$  is

$$\partial_{\sigma_{(i)}} \phi(\boldsymbol{\sigma}) = \frac{3}{2} \partial_{\sigma_e} \phi(\sigma_e) \frac{\sigma_{(i)}}{\sigma_e}. \quad (31)$$

Finally, the spatial average over phase ( $r$ ) of the potential of the relaxation mechanism is given by

$$\langle \phi(\boldsymbol{\sigma}) \rangle \approx \text{stat}_{\beta_{(i)}} \left\{ \frac{1}{2} \sum_{i=1}^5 [\beta_i \langle \sigma_{(i)}^2 \rangle + d_{(i)} (\bar{\sigma}_{(i)} - \hat{\sigma}_{(i)})] + (\phi - \psi)(\hat{\boldsymbol{\sigma}}) \right\}. \quad (32)$$

Here  $\bar{\sigma}_{(i)} = \langle \sigma_{(i)} \rangle$ , and the stationarity condition with respect to  $\beta_{(i)}$  leads to

$$\langle (\sigma_{(i)} - \bar{\sigma}_{(i)})^2 \rangle = (\hat{\sigma}_{(i)} - \bar{\sigma}_{(i)})^2 \quad (33)$$

and the conditions (30) give

$$\beta_{(i)} = \frac{\partial_{\sigma_{(i)}} \phi(\hat{\sigma}_{(i)}) - \partial_{\sigma_{(i)}} \phi(\bar{\sigma}_{(i)})}{\hat{\sigma}_{(i)} - \bar{\sigma}_{(i)}} \quad \text{and} \quad d_{(i)} = \partial_{\sigma_{(i)}} \phi(\hat{\boldsymbol{\sigma}}) - \beta_{(i)} \hat{\sigma}_{(i)}. \quad (34)$$

### 2.4.3. The homogenization procedure

The various linearizations recalled before are applied in the expression of the effective potential (6). Interchanging the stationarity operations with respect to the stress  $\boldsymbol{\sigma}$  and the variables  $\alpha_{(k)}^{(r)}$  and  $\beta_{(i)}^{(r)}$  leads to the approximation of effective stress potential

$$\tilde{U}(\boldsymbol{\sigma}) \approx \text{stat}_{\alpha_{(k)}^{(r)}, \beta_{(i)}^{(r)}} e_{(k)}^{\text{rstat}} d_{(i)}^{(r)} \left\{ \tilde{U}_L(\boldsymbol{\sigma}) - \sum_{r=1}^N c^{(r)} V^{(r)} \right\} \quad (35)$$

where the rstat operation is used to enforce the conditions (22), (30) to determine the parameter  $e_{(k)}^{(r)}$  and  $d_{(i)}^{(r)}$ .  $V^{(r)}$  is independent of the stress tensor  $\boldsymbol{\sigma}$ , its expression is

$$V^{(r)} = \text{stat}_{\hat{\tau}_{(k)}^{(r)}, \hat{\sigma}_{(i)}^{(r)}} \left\{ \sum_{k=1}^K \left[ u_L^{(r)}(\hat{\tau}_{(k)}^{(r)}) - \phi_{(k)}^{(r)}(\hat{\tau}_{(k)}^{(r)}) \right] + \left[ u_L^{(0)}(\hat{\sigma}_e^{(r)}) - \phi_{(i)}^{(r)}(\hat{\sigma}_e^{(r)}) \right] \right\} \quad (36)$$

and

$$\tilde{U}_L(\boldsymbol{\sigma}) = \text{stat}_{\boldsymbol{\sigma} \in \mathcal{S}(\boldsymbol{\sigma})} \langle u_L(\boldsymbol{x}, \boldsymbol{\sigma}) \rangle = \text{stat}_{\boldsymbol{\sigma} \in \mathcal{S}(\boldsymbol{\sigma})} \left\{ \sum_{r=1}^N c^{(r)} \langle u_L^{(r)}(\boldsymbol{\sigma}) \rangle^{(r)} \right\}. \quad (37)$$

The approximation (35) implies that the estimates of effective potential  $\tilde{U}_L$  of the NPLCP may be used to generate corresponding estimates of effective potential  $\tilde{U}$  of the original nonlinear polycrystal. The effective behavior and field statistics in the nonlinear polycrystal are given by those in the NPLCP plus certain ‘‘correction’’ terms (Idiart and Ponte Castañeda, 2005). As mentioned earlier, for the sake of numerical tractability, these ‘‘correction’’ terms are neglected here.

The parameters  $\alpha_{(k)}^{(r)}$ ,  $\beta_{(i)}^{(r)}$ ,  $e_{(k)}^{(r)}$  and  $d_{(i)}^{(r)}$  are given by the optimality conditions (24), (25) and (33), (34). Moreover, the covariance tensor of stress fluctuations  $\underset{\approx}{\boldsymbol{\zeta}}_{\boldsymbol{\sigma}}^{(r)}$  inside the phase ( $r$ ) of NPLCP is directly linked with optimality conditions (25), (34)

$$(\hat{\tau}_{(k)}^{(r)} - \bar{\tau}_{(k)}^{(r)})^2 = \langle (\tau_{(k)}^{(r)} - \bar{\tau}_{(k)}^{(r)})^2 \rangle^{(r)} = \boldsymbol{\mu}_{(k)}^{(r)} : \underset{\approx}{\boldsymbol{\zeta}}_{\boldsymbol{\sigma}}^{(r)} : \boldsymbol{\mu}_{(k)}^{(r)} \quad (38)$$

$$(\hat{\sigma}_{(i)}^{(r)} - \bar{\sigma}_{(i)}^{(r)})^2 = \langle (\sigma_{(i)}^{(r)} - \bar{\sigma}_{(i)}^{(r)})^2 \rangle^{(r)} = \boldsymbol{a}_{(i)}^{(r)} : \underset{\approx}{\boldsymbol{\zeta}}_{\boldsymbol{\sigma}}^{(r)} : \boldsymbol{a}_{(i)}^{(r)} \quad (39)$$

where, for consistency, the positive (negative) value of  $\hat{\tau}_{(k)}^{(r)}$  and  $\hat{\sigma}_{(i)}^{(r)}$  in relation (38) and (39) should be selected for  $\bar{\tau}_{(k)}^{(r)}$  and  $\bar{\sigma}_{(i)}^{(r)}$  positive (negative).

### 2.4.4. On the choice of deviatoric tensor basis

The choice of orthonormal basis for expressing the deviatoric tensors has not been discussed yet. The first naive choice is a fixed basis independent of phases and fields statistics, denoted the ‘fixed basis’ model (FB SO Model). Tensors  $\boldsymbol{a}_i^{(r)}$  introduced in Eqs. (18)–(19) are identified to the deviatoric symmetric tensors, for instance Lequeu's basis  $\{\boldsymbol{a}_i\}$  recalled in Appendix B (Lequeu et al., 1987). As it will be seen below, the FB SO model introduces an artificial anisotropy. The second choice is the eigentensor basis of  $\underset{\approx}{\boldsymbol{\zeta}}_{\boldsymbol{\sigma}}^{(r)}$ . This is the solution that was proposed by Idiart et al. (2006) in a case for which the



principal directions could be known in advance. Doing so, the maximum information of local field statistics is used. However, using this ‘mobile basis’ model (MB SO Model), the necessary eigen-decomposition within the linearization step is harmful to the attractive fixed-point algorithm convergence (see Section 3.1).

To illustrate these issues, we consider a two-phase composite with an isotropic microstructure and phases characterized by a single isotropic and incompressible power-law behavior

$$u^{(r)}(\boldsymbol{\sigma}) = \phi^{(r)}(\sigma_e) = \frac{\sigma_0^{(r)}}{n+1} \left( \frac{\sigma_e}{\sigma_0^{(r)}} \right)^{n+1}. \quad (40)$$

We consider a stress sensitivity  $n=3.5$  and a reference stress contrast  $\sigma_0^{(2)}/\sigma_0^{(1)} = 10$ . The effective behavior of such a composite is isotropic as well. Computations have been performed for three different strain-rate directions:

$$\boldsymbol{\varepsilon}_1 = \varepsilon_e \sqrt{\frac{3}{2}} \boldsymbol{\alpha}_1; \quad \boldsymbol{\varepsilon}_2 = \varepsilon_e \frac{\sqrt{3}}{2} (\boldsymbol{\alpha}_1 + \boldsymbol{\alpha}_2); \quad \boldsymbol{\varepsilon}_3 = \varepsilon_e \sqrt{\frac{3}{10}} (\boldsymbol{\alpha}_1 + \boldsymbol{\alpha}_2 + \boldsymbol{\alpha}_3 + \boldsymbol{\alpha}_4 + \boldsymbol{\alpha}_5)$$

all corresponding to the same equivalent effective strain-rate  $\bar{\varepsilon}_e = \sqrt{\frac{2}{3} \boldsymbol{\varepsilon} : \boldsymbol{\varepsilon}} = 1$ . As for the MB SO model, the numerical convergence of the fixed point algorithm could not be reached when new eigen-vectors were calculated within the convergence loop; we therefore used an approximate solution in which the eigen-vectors were calculated only once, at the beginning of the convergence process. Fig. 1a shows the evolution of normalized equivalent macroscopic stress  $\bar{\sigma}_e/\sigma_0^{(1)}$  vs. the volume fraction  $c^{(2)}$  of phase (2). Results of FB SO and MB SO models are compared with those of the reference second order estimation from Idiart and Ponte Castañeda (2005) (IPC SO Model), which is isotropic by construction (in the IPC SO model, the principal axes of the compliance tensor of the linear comparison composite  $\boldsymbol{M}^{(r)}$  in the phase ( $r$ ) are aligned with the average stress  $\bar{\boldsymbol{\sigma}}^{(r)}$  inside each phase; the linearization thus follows the macroscopic loading direction  $\bar{\boldsymbol{\sigma}}$ ). For the first loading direction aligned with the tensor axes  $\boldsymbol{\alpha}_1$ , all models give very similar responses. For other loading directions, which are linear combinations of tensor axes  $\boldsymbol{\alpha}_i$ , the results of MB SO model well match the reference predictions of IPC SO Model. On the contrary, the FB SO Model underestimates  $\bar{\sigma}_e/\sigma_0^{(1)}$ . This model also artificially introduces a mechanical anisotropy, as evidenced in Fig. 1b where the evolution of the intra-phase heterogeneity of stress for phase 1,  $\omega_\sigma^{(1)} = \sqrt{\langle \sigma_e^2 \rangle^{(1)} / \bar{\sigma}_e^{(1)}}$  is plotted as a function of  $c^{(2)}$ : results depend on the loading direction. The introduction of a fixed basis for the linearization does not allow to using the complete statistical informations contained inside the covariance tensor of stress fluctuations  $\boldsymbol{\zeta}_{\boldsymbol{\sigma}}^{(r)}$ . Finally, the requirement of isotropy imposes an eigen-decomposition of  $\boldsymbol{\zeta}_{\boldsymbol{\sigma}}^{(r)}$  for the SO extension of SC scheme, which is an issue for numerical convergence.

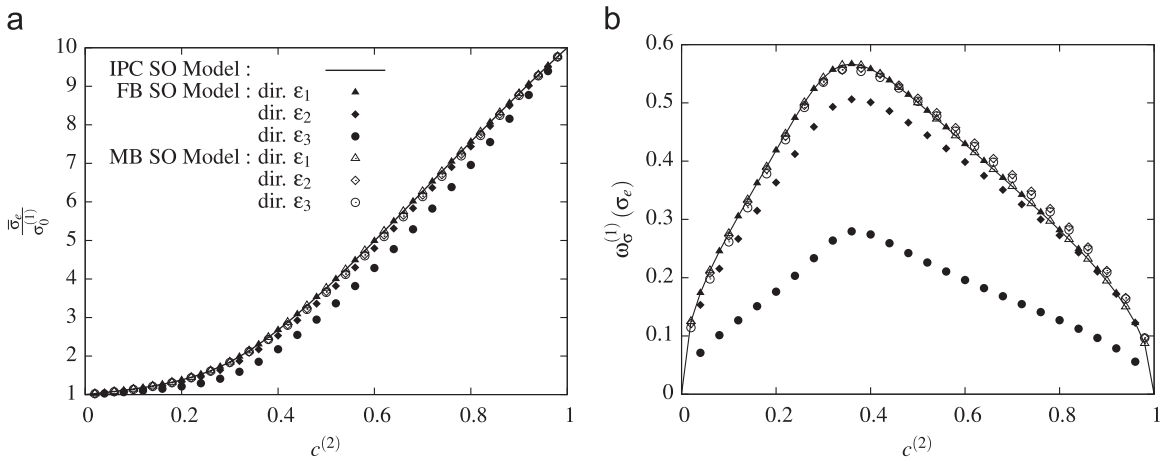


**Fig. 1.** Influence of loading directions  $\boldsymbol{\varepsilon}_i$  for two choices of the tensor basis (FB SO and MB SO) used within the framework of the Second Order extensions of the SC estimate on (a) the normalized equivalent macroscopic stress  $\bar{\sigma}_e/\sigma_0^{(1)}$  and (b) the intra-phase heterogeneity of stress  $\omega_\sigma$  for phase (1), as a function of the volume fraction  $c^{(2)}$  of the second phase, with a reference stress contrast  $\sigma_0^{(2)}/\sigma_0^{(1)} = 10$  and a stress sensitivity  $n=3.5$ . Reference results of the second order estimate of Idiart and Ponte Castañeda (2005) (IPC) are also indicated.

## 2.5. New second order linearization estimate for the isotropic potential

In this section, instead of using directly the isotropic potential  $\phi_{(0)}(\sigma_e)$  as in previous Sections 2.4.2 and 2.4.4, with associated isotropy and numerical issues, we make use of an approximation of this potential, ensuring isotropy and rapid numerical convergence of the homogenization code. To that end,  $\phi_{(0)}(\sigma_e)$  is decomposed into a sum of potentials associated to fictitious deformation mechanisms which ‘orientation’ are fixed with respect to the crystal (as for slip systems). Note however that it is impossible to decompose an isotropic incompressible potential as a sum of slip system potentials; but in a special case of a (two-phase) porous material subjected to anti-plane loadings, the isotropic potential can be decomposed as a sum of slip system potentials, as shown by [Idiart and Ponte Castañeda \(2007\)](#).

In a more general case, the isotropic potential can be written as an integral over the space of deviatoric symmetric unit tensors ( $\mathbb{S}^4$ ):

$$\phi_{(0)}(\sigma_e) = \frac{\sigma_0 \dot{\epsilon}_0}{n_{(0)} + 1} \left( \frac{\sigma_e}{\sigma_0} \right)^{n_{(0)}+1} = \int_{\mathbb{S}^4} \bar{\varphi}(\sigma_k) d\mathbf{k}, \quad \sigma_k = \boldsymbol{\varepsilon} : \mathbf{k} \quad (41)$$

where  $\mathbb{S}^4$  is isomorphic to unit sphere of  $\mathbb{R}^5$ ,  $\mathbf{k}$  is a unit deviatoric symmetric tensor and  $\bar{\varphi}(\sigma_k)$  has a similar form as a slip system potential:

$$\bar{\varphi}(\sigma_k) = \varrho[n_{(0)}] \frac{\sigma_0 \dot{\epsilon}_0}{n_{(0)} + 1} \left| \frac{\sigma_k}{\sigma_0} \right|^{n_{(0)}+1} \quad (42)$$

with the normalization constant  $\varrho[n_{(0)}] = (n_{(0)} + 4)(n_{(0)} + 2)/8\pi^2$ . The above continuous integral on  $\mathbb{S}^4$  can be approximated by its discretized expression

$$\phi_{(0)}(\sigma_e) = \int_{\mathbb{S}^4} \bar{\varphi}(\boldsymbol{\varepsilon} : \mathbf{k}) d\mathbf{k} \approx \sum_{p=1}^P C_{(p)} \bar{\varphi}(\sigma_{(p)}) \quad (43)$$

where  $\sigma_{(p)} = \boldsymbol{\varepsilon} : \mathbf{k}_{(p)}$  is the projection of stress tensor  $\boldsymbol{\varepsilon}$  over the nodes  $\mathbf{k}_{(p)}$  associated to the integral discretization and  $C_{(p)}$  is the corresponding integration weight. So the potential  $\phi_{(0)}(\sigma_e)$  is approximated by a sum of potentials  $\bar{\varphi}_{(p)}^{(r)} = C_{(p)} \bar{\varphi}(\sigma_{(p)})$  having a similar form as a standard slip system potential. But note that these potentials differ from real slip systems since  $\mathbf{k}$  does not have the shape of a Schmid tensor. Note also that the activation of the accommodation mechanism does not generate any evolution of the crystallographic texture, unlike dislocation slip systems (see Section 4.5).

The linearized potential used in the following is based on the present approximation and it is built by a linearization of each potential  $\bar{\varphi}_{(p)}^{(r)}$ :

$$u_L^{(r)}(\boldsymbol{\varepsilon}) = \sum_{p=1}^P \left[ \frac{1}{2} \beta_{(p)} \sigma_{(p)}^2 + d_{(p)} \sigma_{(p)} \right]. \quad (44)$$

The same approximation introduced by [Liu and Ponte Castañeda \(2004\)](#) and used for slip systems (Section 2.4.1) is also used for the spatial average of the potential  $\bar{\varphi}_{(p)}^{(r)}$ :

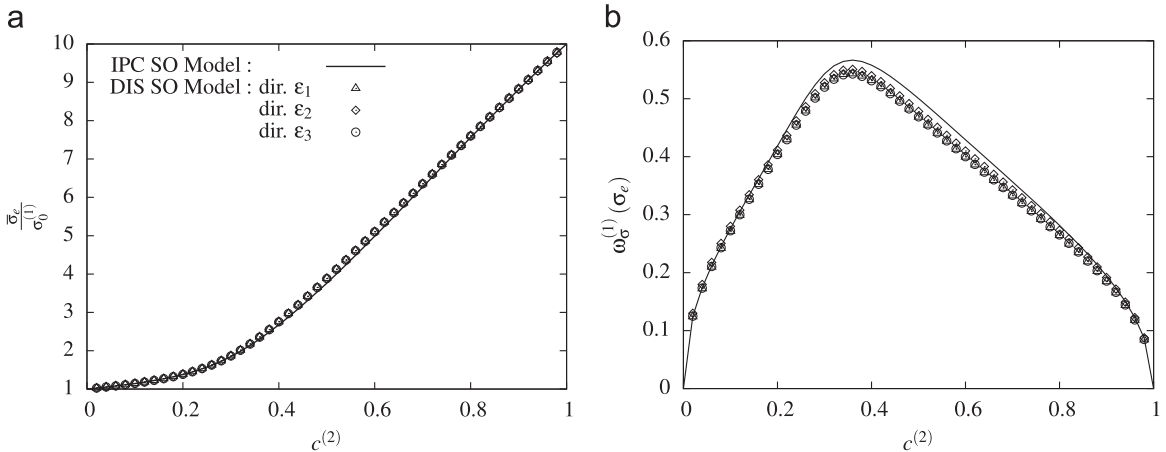


**Fig. 2.** Influence of the loading direction  $\varepsilon_i$  on (a) the normalized equivalent macroscopic stress  $\bar{\sigma}_e/\sigma_0^{(1)}$  and (b) the intra-phase stress heterogeneity  $\omega_\sigma(1)$  in phase (1), as a function of the volume fraction  $c^{(2)}$ , with a mechanical contrast  $\sigma_0^{(2)}/\sigma_0^{(1)} = 10$  and a stress sensitivity  $n = 3.5$ . The discretized Second Order (DIS SO) extension of the SC scheme is compared to the reference results of [Idiart and Ponte Castañeda \(2005\)](#).

$$\langle \bar{\varphi}_{(p)}(\sigma_{(p)}) \rangle^{(r)} \approx \text{stat} \left\{ \frac{1}{\beta_{(p)}} \langle \sigma_{(p)}^2 \rangle^{(r)} + d_{(p)}(\sigma_{(p)} - \hat{\tau}_{(p)}) + \phi_{(p)}(\hat{\tau}_{(p)}) - \frac{1}{2\beta_{(p)}} \hat{\tau}_{(p)}^2 \right\} \quad (45)$$

where  $\bar{\sigma}_{(p)}^{(r)} = \langle \sigma_{(p)} \rangle^{(r)}$  and  $\beta_{(p)}$ ,  $d_{(p)}$  and  $\hat{\tau}_{(p)}$  are given by

$$\beta_{(p)} = \frac{\partial_{\sigma_{(p)}} \varphi_{(p)}(\hat{\sigma}_{(p)}) - \partial_{\sigma_{(p)}} \varphi_{(p)}(\bar{\sigma}_{(p)})}{\hat{\sigma}_{(p)} - \bar{\sigma}_{(p)}} \quad \text{and} \quad d_{(p)} = \partial_{\sigma_{(p)}} \varphi_{(p)}(\hat{\sigma}_{(p)}) - \beta_{(p)} \hat{\sigma}_{(p)}, \quad (46)$$

$$(\hat{\sigma}_{(p)} - \bar{\sigma}_{(p)})^2 = \langle (\sigma_{(p)} - \bar{\sigma}_{(p)})^2 \rangle^{(r)} = \mathbf{k}_{(p)}^{(r)} : \underset{\approx}{\mathbf{C}}_{\mathbf{e}}^{(r)} : \mathbf{k}_{(p)}^{(r)}. \quad (47)$$

Note that, for consistency, the positive (negative) value of  $\hat{\sigma}_{(p)}$  in the relation (47) should be selected for  $\bar{\sigma}_{(p)}^{(r)}$  positive (negative).

The quality of this discretized second-order estimation (DIS SO Model) depends on the quality of the integral approximation (43). The details of this discretization into 1073 potentials are given in Section 3.2. Fig. 2 shows the good agreement between DIS SO and the reference IPC SO model, and the very good respect of isotropy requirement, which is an improvement over the FB SO model. Moreover the convergence of the point-fixed algorithm is ensured unlike the MB SO model.

### 3. Algorithmic setting of the constitutive model

#### 3.1. Attractive fixed-point algorithm

Under these assumptions, the set of nonlinear equations to compute the statistics of local fields and the macroscopic response could be summarized for all linearization schemes by

$$\left\{ \begin{array}{l} \text{Localization procedure} \\ \forall r \quad \mathbf{t}^{(r)} = \langle \boldsymbol{\sigma} \rangle^{(r)} = \underline{\mathbf{B}}^r(c^{(s)}, \underline{\mathbf{M}}^{(s)}, \underline{\mathbf{e}}^{(s)}, \dots) : \bar{\boldsymbol{\sigma}} + \underline{\mathbf{b}}^{(r)}(c^{(s)}, \underline{\mathbf{M}}^{(s)}, \underline{\mathbf{e}}^{(s)}, \dots) \\ \text{Second order moment} \\ \forall r \quad \underline{\mathbf{T}}^{(r)} = \langle \boldsymbol{\sigma} \otimes \boldsymbol{\sigma} \rangle^{(r)} = \underline{\mathbf{T}}^{(r)}(\langle \boldsymbol{\sigma} \rangle^{(r)}; c^{(s)}, \underline{\mathbf{M}}^{(s)}, \underline{\mathbf{e}}^{(s)}, \dots) \\ \text{Linearization procedure} \\ \forall r \quad \underline{\mathbf{M}}^{(r)} = \underline{\mathbf{M}}^{(r)}(\mathbf{t}^r, \underline{\mathbf{T}}^{(r)}) \quad \text{and} \quad \underline{\mathbf{e}}^{(r)} = \underline{\mathbf{e}}^{(r)}(\mathbf{t}^r, \underline{\mathbf{T}}^{(r)}) \\ \text{Microscopic response} \\ \forall r \quad \bar{\boldsymbol{\sigma}}^{(r)} = \underline{\mathbf{M}}^{(r)}(c^{(s)}, \underline{\mathbf{M}}^{(s)}, \underline{\mathbf{e}}^{(s)}, \dots) : \bar{\boldsymbol{\sigma}}^{(r)} + \underline{\mathbf{e}}^{(r)}(c^{(s)}, \underline{\mathbf{M}}^{(s)}, \underline{\mathbf{e}}^{(s)}, \dots) \\ \text{Macroscopic response} \\ \bar{\boldsymbol{\sigma}} = \underline{\mathbf{M}}(c^{(s)}, \underline{\mathbf{M}}^{(s)}, \underline{\mathbf{e}}^{(s)}, \dots) : \bar{\boldsymbol{\sigma}} + \underline{\tilde{\mathbf{e}}}(c^{(s)}, \underline{\mathbf{M}}^{(s)}, \underline{\mathbf{e}}^{(s)}, \dots) \end{array} \right.$$

An iterative algorithm is used to solve this system of nonlinear equations. The macroscopic strain-rate ( $\bar{\boldsymbol{\epsilon}}$ ) and the statistics of local fields ( $\bar{\boldsymbol{\sigma}}^{(r)}$ ,  $\bar{\boldsymbol{\sigma}}^{(r)}$ ;  $\langle \boldsymbol{\sigma} \otimes \boldsymbol{\sigma} \rangle^{(r)}$ , ...), which are associated to the macroscopic stress ( $\bar{\boldsymbol{\sigma}}$ ), are computed by an attractive fixed-point algorithm described in Table 2. In Table 2, the macroscopic stress tensor is prescribed, but the algorithm can be easily modified for a prescribed macroscopic strain-rate, or for mixed stress/strain-rate inputs.

The initialization step is of paramount importance for attractive fixed-point algorithm convergence. A uniform stress state (static bound) is used for SEC, AFF, TGT extensions of SC estimate while the solution of AFF (respectively SEC) model is used for SO (respectively VAR) extension of SC estimate.

Convergence is attained when all four errors  $\{\epsilon_1, \epsilon_2, \epsilon_3, \epsilon_4\}$  are smaller than a given threshold  $\epsilon^0$  (typically taken equal to  $10^{-4}$ ). The two first errors ( $\epsilon_1, \epsilon_2$ ) ensure that the averages of local fields converge toward the macroscopic fields, whereas the next two errors ( $\epsilon_3, \epsilon_4$ ) ensure the solution stability. Here, the stability implies that, when the solution local fields are reused in the linearization step, the same local fields are found after the homogenization process. The norm  $\|\cdot\|_{\infty}$  of deviatoric tensor is used to define errors:

$$\|\underline{\mathbf{t}}\|_{\infty} = \max_{1 \leq i \leq 5} \{ |t_i| \} \quad \text{with} \quad \underline{\mathbf{t}} = \sum_{i=1}^5 t_i \boldsymbol{\alpha}_i \quad (48)$$

where  $\{\boldsymbol{\alpha}_1, \dots, \boldsymbol{\alpha}_5\}$  is Lequeu's orthonormal basis of deviatoric tensors (Appendix B). This definition is extended to fourth-order tensor such as  $\underline{\mathbf{T}} = \sum_{i,j=1}^5 T_{ij} \boldsymbol{\alpha}_i \otimes \boldsymbol{\alpha}_j$  and  $T_{ij} = T_{ji}$ , by

$$\|\underline{\mathbf{T}}\|_{\infty} = \max_{1 \leq i, j \leq 5} \{ |T_{ij}| \}. \quad (49)$$

**Table 2**  
Implementation of the homogenization model.

---

1.	Initialization: $\forall r \mathbf{t}^{(r)} \leftarrow \bar{\mathbf{t}}_{ini}^{(r)}; \mathbf{T}^{(r)} \leftarrow \langle \boldsymbol{\varepsilon} \otimes \boldsymbol{\varepsilon} \rangle_{ini}^{(r)}$
2.	<p><b>WHILE</b> <math>\max(\epsilon_1, \epsilon_2, \epsilon_3, \epsilon_4) \geq \epsilon^0</math> (convergence criteria)</p> <p>(a) Linearization process</p> $\forall r \mathbf{M}^{(r)} \leftarrow \underline{\underline{\mathbf{M}}}^{(r)}(\mathbf{t}^r, \mathbf{T}^{(r)}); \quad \boldsymbol{\varepsilon}^{(r)} \leftarrow \boldsymbol{\varepsilon}^{(r)}(\mathbf{t}^r, \mathbf{T}^{(r)})$ <p>(b) Localization process</p> $\forall r \bar{\boldsymbol{\varepsilon}}^{(r)} \leftarrow \mathbf{B}^r(c^{(s)}, \underline{\underline{\mathbf{M}}}^{(s)}, \boldsymbol{\varepsilon}^{(s)}, \dots); \bar{\mathbf{b}}^{(r)}(c^{(s)}, \underline{\underline{\mathbf{M}}}^{(s)}, \boldsymbol{\varepsilon}^{(s)}, \dots)$ <p>(c) Compute field statistics</p> $\bar{\boldsymbol{\varepsilon}} \leftarrow \bar{\underline{\underline{\mathbf{M}}}}(c^{(s)}, \underline{\underline{\mathbf{M}}}^{(s)}, \boldsymbol{\varepsilon}^{(s)}, \dots); \bar{\boldsymbol{\varepsilon}} + \tilde{\boldsymbol{\varepsilon}}(c^{(s)}, \underline{\underline{\mathbf{M}}}^{(s)}, \boldsymbol{\varepsilon}^{(s)}, \dots) \quad (\text{effective})$ $\forall r \bar{\boldsymbol{\varepsilon}}^{(r)} \leftarrow \underline{\underline{\mathbf{M}}}^{(r)}(\mathbf{t}^r, \mathbf{T}^{(r)}); \bar{\boldsymbol{\varepsilon}}^{(r)} + \boldsymbol{\varepsilon}^{(r)}(\mathbf{t}^r, \mathbf{T}^{(r)}) \quad (\text{1st moments})$ $\forall r \langle \boldsymbol{\varepsilon} \otimes \boldsymbol{\varepsilon} \rangle^{(r)} \leftarrow \mathbf{T}^{(r)}(\bar{\boldsymbol{\varepsilon}}^{(r)}; c^{(s)}, \underline{\underline{\mathbf{M}}}^{(s)}, \boldsymbol{\varepsilon}^{(s)}, \dots) \quad (\text{2nd moments})$ <p>(d) Compute error criterion</p> $\epsilon_1 = \frac{\ \bar{\boldsymbol{\varepsilon}} - \sum c^r \bar{\boldsymbol{\varepsilon}}^{(r)}\ _{\infty}}{\ \bar{\boldsymbol{\varepsilon}}\ _{\infty}}; \quad \epsilon_2 = \frac{\ \bar{\boldsymbol{\varepsilon}} - \sum c^r \bar{\boldsymbol{\varepsilon}}^{(r)}\ _{\infty}}{\ \bar{\boldsymbol{\varepsilon}}\ _{\infty}}$ $\epsilon_3 = \max_{(r)} \left\{ \frac{\ \mathbf{t}^{(r)} - \bar{\mathbf{t}}^{(r)}\ _{\infty}}{\ \bar{\mathbf{t}}\ _{\infty}} \right\}; \quad \epsilon_4 = \max_{(r)} \left\{ \frac{\ \mathbf{T}^{(r)} - \langle \boldsymbol{\varepsilon} \otimes \boldsymbol{\varepsilon} \rangle^{(r)}\ _{\infty}}{\ \langle \boldsymbol{\varepsilon} \otimes \boldsymbol{\varepsilon} \rangle^{(r)}\ _{\infty}} \right\}$ <p>(e) Local variables updating</p> $\forall r \mathbf{t}^{(r)} \leftarrow \theta \bar{\mathbf{t}}^{(r)} + (1 - \theta) \mathbf{t}^{(r)} \quad \text{with } \theta \in [0; 1]$ $\forall r \mathbf{T}^{(r)} \leftarrow \theta \langle \boldsymbol{\varepsilon} \otimes \boldsymbol{\varepsilon} \rangle^{(r)} + (1 - \theta) \mathbf{T}^{(r)}$
3.	Postprocessing

---

The adaptive parameter  $\theta$  regulates the convergence rate of attractive fixed-point algorithm. The  $\theta$  value is automatically updated according to error variations to ensure convergence.

In the post-processing step, activities of deformation mechanisms (Section 4.4) and some statistical fields, such as  $\langle \boldsymbol{\varepsilon} \otimes \boldsymbol{\varepsilon} \rangle^{(r)}$ , are computed. The phase orientations  $\underline{\underline{\mathbf{Q}}}_{\Delta t}^{(r)}$  are also updated after a given step time  $\Delta t$  by assuming uniform lattice rotation-rates  $\underline{\underline{\mathbf{Q}}}^{(r)}$  over the  $r$ th phase

$$\underline{\underline{\mathbf{Q}}}^{(r)} = \underline{\underline{\mathbf{Q}}}_{\text{ellipsoid}}^{(r)} - \underline{\underline{\mathbf{Q}}}_p^{(r)} \quad (50)$$

where  $\underline{\underline{\mathbf{Q}}}_{\text{ellipsoid}}^{(r)}$  is rotation-rate tensor of the ellipsoidal domain associated to the phase ( $r$ ), given e.g. in Lebensohn et al. (2011), and  $\underline{\underline{\mathbf{Q}}}_p^{(r)}$  is the plastic rotation-rate tensor

$$\underline{\underline{\mathbf{Q}}}_p^{(r)} = \sum_{k=1}^N \dot{\gamma}_{(k)}^{(r)} \frac{1}{2} \left( \mathbf{n}_{(k)}^{(r)} \otimes \mathbf{m}_{(k)}^{(r)} - \mathbf{m}_{(k)}^{(r)} \otimes \mathbf{n}_{(k)}^{(r)} \right) \quad (51)$$

with the slip-rate  $\dot{\gamma}_{(k)}^{(r)}$  on slip system ( $k$ ) in the phase ( $r$ ). Note that strain due to activation of the accommodation mechanism (corresponding to  $k=0$  in the above equation) does not induce any plastic rotation. Texture evolution of polycrystals along a given strain path can be computed by using this algorithm successively along different strain increments. Finally, the shape of ellipsoidal inclusions is updated with respect to the increment of the macroscopic deformation gradient  $\Delta \bar{\mathbf{F}}^t = \Delta t \bar{\mathbf{L}}^t$ .  $\bar{\mathbf{F}}^t$  obtained by an explicit approximation of macroscopic velocity gradient tensor  $\bar{\mathbf{L}}^t$ .

### 3.2. Discretization of isotropic incompressible potential

The accuracy of this discretized second-order estimation (DIS SO Model) depends on the quality of the integral approximation (43). A decomposition of the integral defined on  $\mathbb{S}^4$  in two successive integrals defined on the surface sphere  $\mathbb{S}^2$  is used in order to apply the efficient numerical integration developed by [Bazant and Oh \(1986\)](#). The method requires fewer integration points than the classical Gauss approximation for a same degree of approximation; and moreover, it gives the smallest difference between minimal and maximal values of integrals for all directions of  $\boldsymbol{\sigma}$ .

Consider a unit deviatoric symmetric tensor  $\boldsymbol{k} = (k_1, \dots, k_5)$  in Lequeu's tensor basis. Its components can be described by a generalized system of spherical coordinates  $\{\theta_1, \theta_2, \theta_3, \theta_4\}$ :

$$\begin{aligned} k_1 &= \cos(\theta_4)\cos(\theta_3)\cos(\theta_2)\cos(\theta_1), & k_2 &= \cos(\theta_4)\cos(\theta_3)\cos(\theta_2)\sin(\theta_1) \\ k_3 &= \cos(\theta_4)\cos(\theta_3)\sin(\theta_2), & k_4 &= \cos(\theta_4)\sin(\theta_3), & k_5 &= \sin(\theta_4). \end{aligned}$$

The symmetry of potential  $\bar{\varphi}(\sigma_k)$  with respect to  $\boldsymbol{k}$  ( $\bar{\varphi}(\sigma_{-k}) = \bar{\varphi}(\sigma_k)$ ) leads to

$$\phi_{(0)}(\sigma_e) = \int_{\mathbb{S}_+^2} \left( \int_{\mathbb{S}_+^2} \bar{\varphi}(\sigma_k) \frac{\pi^2}{3} \cos^2(\theta_3) \cos^2(\theta_4) dm_2 \right) dm_1 \quad (52)$$

where  $\mathbb{S}_+^2$  is the semi-sphere, such as ( $\forall i\theta_i \in [-\pi/2, \pi/2]$ ) and  $dm_1 = \cos(\theta_2) d\theta_1 d\theta_2$  and  $dm_2 = \cos(\theta_4) d\theta_3 d\theta_4$  are the surface elements of  $\mathbb{S}^2$ . A 13th degree approximation with orthogonal symmetries of integral over unit semi-sphere is used:

$$\phi_{(0)}(\sigma_e) \approx \frac{\pi^2}{3} \sum_{n=1}^{37} \sum_{m=1}^{37} C_n C_m^* \bar{\varphi}(\boldsymbol{\sigma} : \boldsymbol{k}^{n,m}) \quad (53)$$

where  $C_n$  and  $C_m^* = C_m \cos^2(\theta_1^n) \cos^2(\theta_2^m)$  are integration weights. The angle  $\theta_i^n$  is the  $n$ th value of the angle  $\theta_i$  and the discretization direction  $\boldsymbol{k}^{n,m}$  corresponds to the unit deviatoric tensor associated to  $(\theta_1^n, \theta_2^m, \theta_1^m, \theta_2^n)$  in the generalized system of spherical coordinates. The values of discretization angles ( $\theta_i^n$ ) and associated weights ( $C_n$ ) are given in [Fig. 3](#).

Note that some weights  $C_m^*$  are vanishing, thus decreasing the number of interpolation points from  $37 \times 37 = 1369$  to 1073. Removing these vanishing terms, a change of indices  $p = (n, m)$  with  $C_{(p)} = (\pi^2/3)C_n C_m^*$  leads to the final expression of potential approximation:

$$\phi_{(0)}(\sigma_e) \approx \sum_{p=1}^{1073} C_{(p)} \bar{\varphi}(\boldsymbol{\sigma} : \boldsymbol{k}_{(p)}). \quad (54)$$

This is not the most powerful approximation: it is possible to find a 13th degree approximation with less interpolation points, for example by generalizing the procedure used by [Bazant and Oh \(1986\)](#). Nevertheless, with a maximal relative error of about  $10^{-4}$  for a nonlinear potential  $n_{(0)} = 3.5$ , it is better than the 13th degree Gauss approximation which has a maximal relative error of the order of about 0.1 for the same potential and with more than twice as many interpolation points ( $7^4 = 2401$ ). Note also that using 1073 interpolation points as in Eq. (54) is not critical for the CPU time, as most of it is spent for integrating the Eshelby tensor and its derivative.

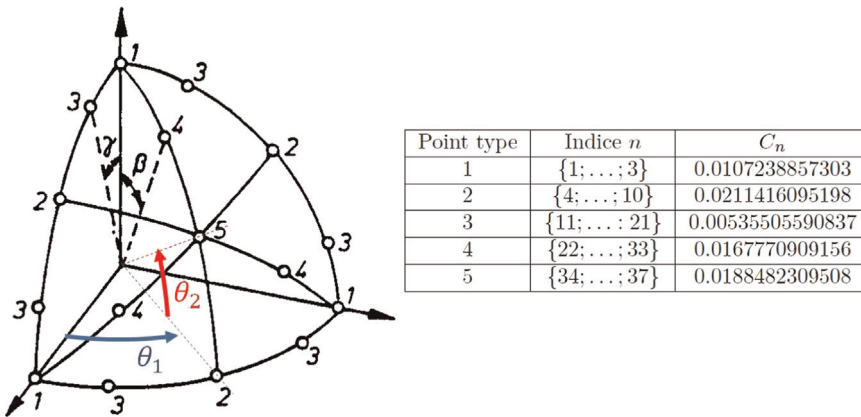


**Fig. 3.** The right table gives the list of integration weights on unit semi-sphere  $\mathbb{S}_+^2$ . The left figure shows the location of integration points on one-eighth of the unit sphere ([Bazant and Oh, 1986](#)). The type 1 points are the intersections of sphere with the axis; the type 2 points are in the middle on the arc between two type 1 points; the positions of types 3 and 4 points are defined by the angles  $\gamma=0.3140901570977$  rad and  $\beta=0.4938054766135$  rad respectively and the type 5 point is the intersection of the arcs between the opposite points of type 1 and type 2. Points on the other semi-sphere are obtained by symmetry.

**Table 3**

Olivine CRSS taken from [Raterron et al. \(2014\)](#) at 360 km depth along a 20 Ma oceanic geotherm. Note that CRSS values are normalized with respect to that of [100](010), that serves as a reference.

Slip system	[100](010)	[001](010)	[001](100)	[100](001)	[100](021)	[001](110)
$\tau_0$	1.00	0.46	1.14	1.40	1.14	1.40

### Nonlinear isotropic relaxation mechanism ( $n_{(0)} = 3.5$ )

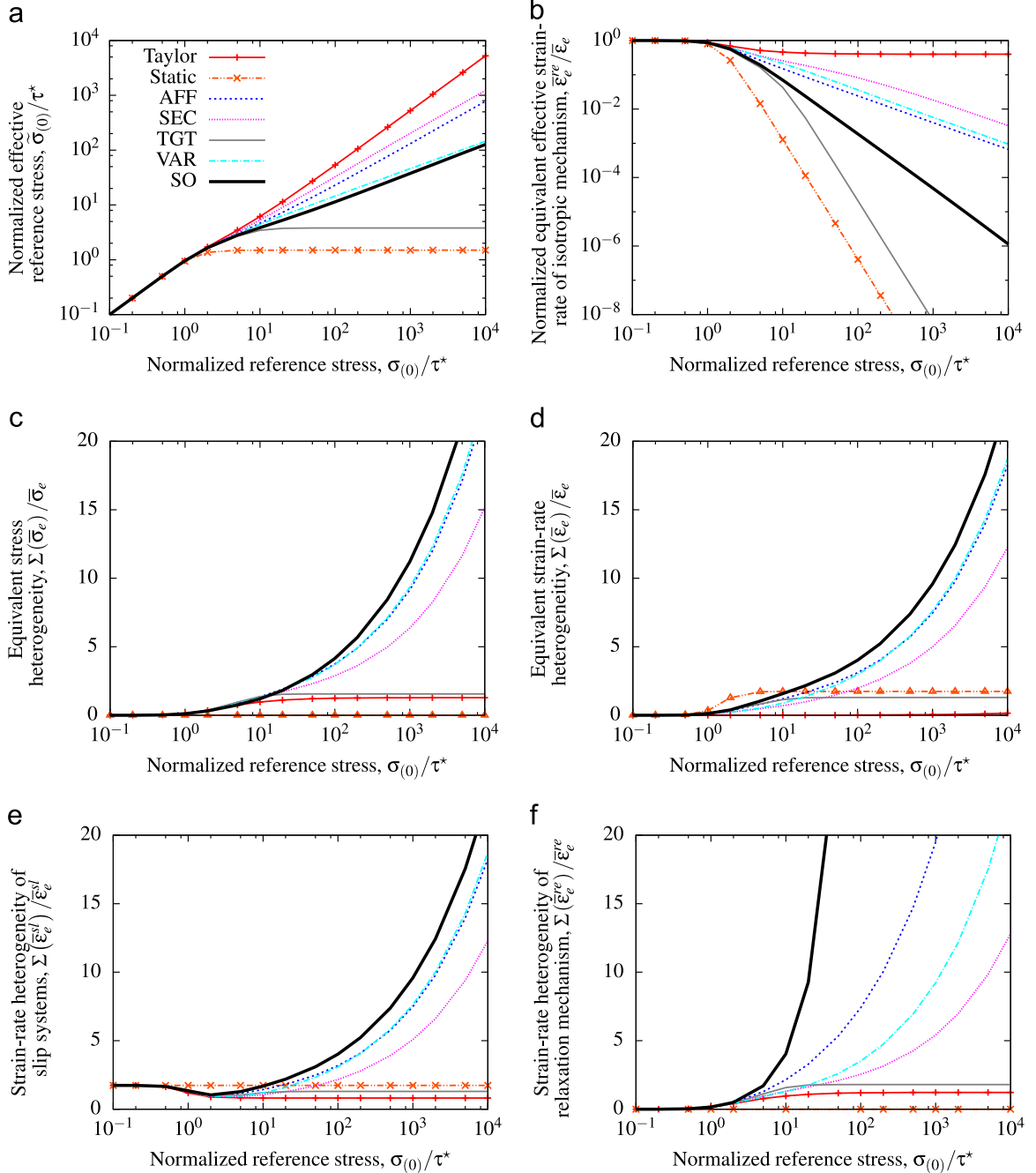


**Fig. 4.** Effect of the normalized reference stress  $\sigma_{(0)}/\tau^*$  for several extensions of the SC scheme. Static and Taylor bounds are also indicated, for comparison.

## 4. Application to olivine aggregates

### 4.1. Constitutive relations

(Mg<sub>0.9</sub>Fe<sub>0.1</sub>)<sub>2</sub>SiO<sub>4</sub> olivine (orthorhombic, space group *Pbnm*) is the main constituent of the Earth's upper mantle and is stable up to pressures and temperatures in excess of 13 GPa and 1760 K. It is an interesting material from a mechanical point of view since it only has six slip system families, listed in Table 3, but only three independent slip systems; therefore an additional plastic relaxation mechanism is required. The lack of slip systems in many mineral phases, including olivine, raises a fundamental question that is usually avoided in the literature, e.g. by using ad hoc micromechanical models, or tackled by introducing artificial slip systems. The real accommodation mechanisms occurring in olivine are largely unknown yet: grain boundary sliding, Coble or Nabarro–Herring diffusion, dislocation climb, or even disclinations as proposed recently by Cordier et al. (2014). The implication of diffusive phenomenon is often involved, e.g. diffusion could be a good candidate for the accommodation of grain-boundary sliding and therefore could control the deformation rate. We are not yet at a stage where these potential mechanisms can be introduced into the SO model. Therefore, for the sake of simplicity, we assume that the unknown accommodation mechanism can be represented by an isotropic potential. This work aims to inferring what could be the effects of accommodation mechanisms in real olivine, in order to provide a guideline for future specific experimental studies.

We assume here that potential  $\phi_{(k)}$  given in Eq. (4) can be used at slip system level, with  $\dot{\gamma}_0 = 10^{-15} \text{ s}^{-1}$  and identical stress sensitivities  $n_{(k)} = 3.5$  for all slip systems (Bai et al., 1991). Accordingly, the slip-rate  $\gamma_{(k)}$  on system ( $k$ ) reads

$$\gamma_{(k)} = \partial_{\tau_{(k)}} \phi_{(k)}(\tau_{(k)}) = \dot{\gamma}_0 \left| \frac{\tau_{(k)}}{(\tau_0)_{(k)}} \right|^{n_{(k)}-1} \frac{\tau_{(k)}}{(\tau_0)_{(k)}} \quad (55)$$

Linear isotropic relaxation mechanism ( $n_{(0)} = 1$ )

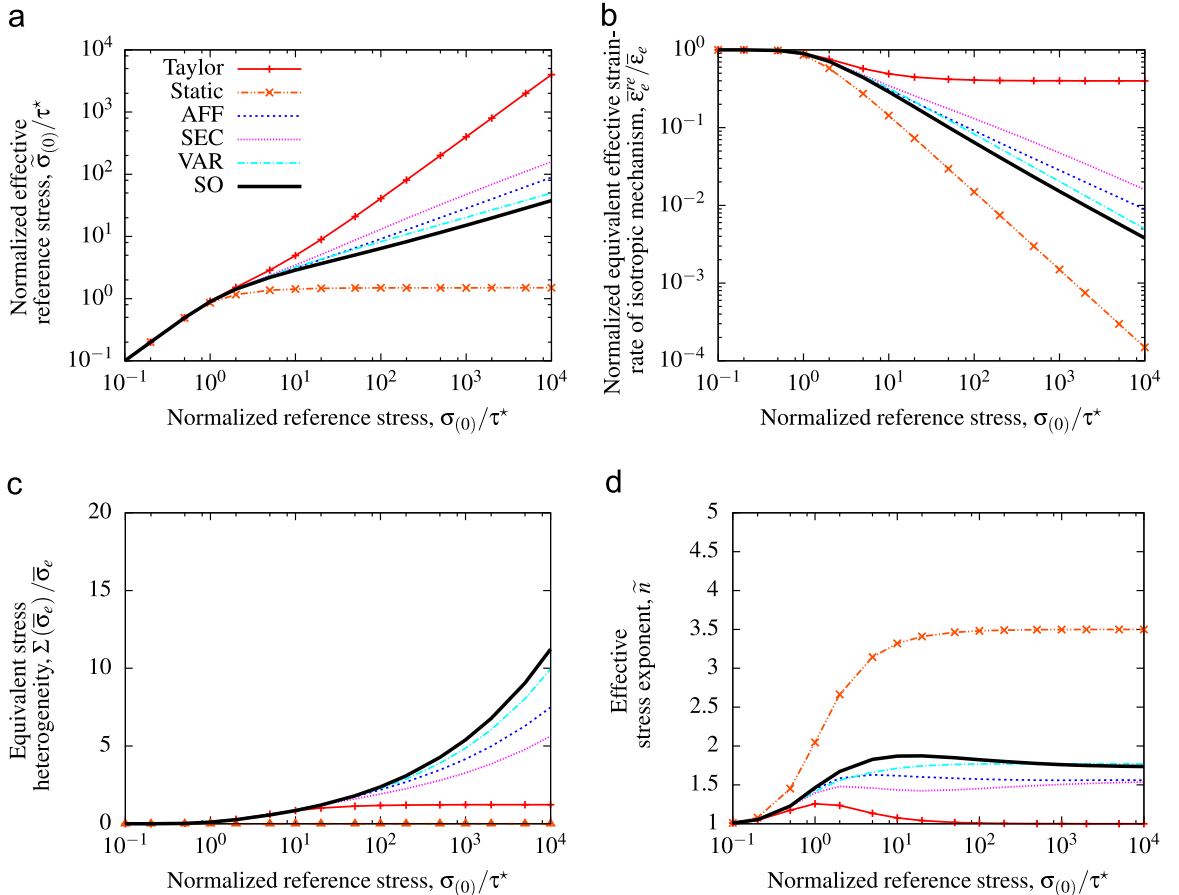


**Fig. 5.** Effect of the reference stress  $\sigma_{(0)}/\tau^*$  for several extensions of the SC scheme, for the case of a linear viscous relaxation mechanism ( $n_{(0)} = 1$ ). Static and Taylor bounds are shown for comparison.

Normalized reference stress  $\sigma_{(0)}/\tau^* = 1000$

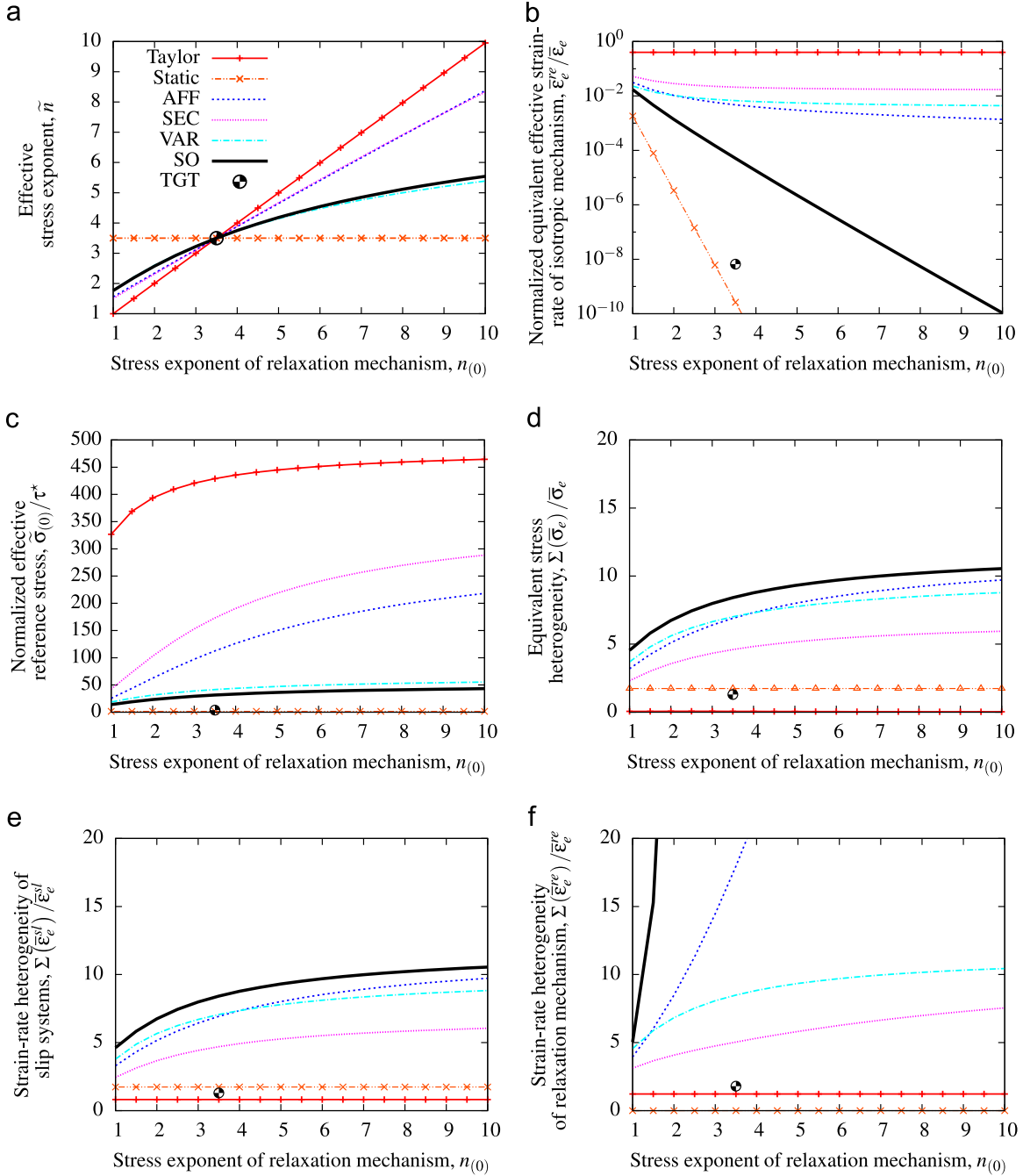


**Fig. 6.** Effect of the stress sensitivity  $n_{(0)}$  of the isotropic relaxation mechanism for several extensions of the SC scheme. Static and Taylor bounds are shown for comparison.

In this section, we investigate the influence of parameters  $n_{(0)}$  and  $\sigma_{(0)}$  of the isotropic relaxation mechanism on the rheology of polycrystalline olivine. The effective polycrystal behavior can be expressed as a power law

$$\frac{\bar{\epsilon}_{eq}}{\bar{\epsilon}_0} = \left( \frac{\sigma_{eq}}{\bar{\sigma}_{(0)}} \right)^{\bar{n}} \quad (56)$$

where  $\bar{n}$  and  $\bar{\sigma}_{(0)}$  are respectively the effective stress sensitivity and reference stress. The reference macroscopic strain-rate  $\bar{\epsilon}_0$



is taken equal to both the reference strain-rate of the relaxation mechanism and the reference shear-rate for slip, i.e.  $\bar{\epsilon}_0 = \epsilon_0 = \dot{\gamma}_0 = 10^{-15} \text{ s}^{-1}$ .

The macroscopic law (56) is an approximation which corresponds to a linearization of  $\ln \bar{\epsilon}_{eq}$  with respect to  $\ln \bar{\sigma}_{eq}$  for geological conditions ( $\bar{\epsilon}_{eq} \approx 10^{-15} \text{ s}^{-1}$ ). Note, however, that the polycrystal macroscopic behavior will not follow a power-law if the relaxation mechanism stress exponent differs from that of the individual slip systems.

We have tested the various extensions of the SC scheme on an olivine polycrystal made of 500 random crystal orientations (or mechanical phases), so that the effective behavior of the polycrystal is isotropic. We perform computations with an effective equivalent strain-rate  $\bar{\epsilon}_e = \epsilon_0$  under uniaxial tension. Results are discussed below.

#### 4.2. Influence of the relative strength of the isotropic relaxation mechanism

In this section, we first consider the case for which all stress sensitivities are identical. Then, we will investigate the effect of having different stress sensitivities.

##### 4.2.1. Case $n_{(0)} = n_{(k)} = 3.5$

In this section, we investigate the effect of the relative strength of the isotropic relaxation mechanism in the case where all deformation mechanisms exhibit the same stress sensitivity  $n_{(0)} = n_{(k)} = 3.5$ . Results are presented in Fig. 4 as a function of  $\sigma_{(0)}/\tau^*$ , where  $\sigma_{(0)}$  is the strength of the isotropic mechanism and  $\tau^* = \sqrt{3/2} \times \tau_{0(100)(010)}$  is a normalization stress. This value of  $\tau^*$  is the stress for which both the isotropic mechanism and slip along  $[100](010)$  have the same strain-rate for a shear stress that is aligned with  $[100](010)$ .

Fig. 4a shows the normalized effective stress  $\bar{\sigma}_{(0)}/\tau^*$  as predicted by the SEC, AFF, TGT, VAR and SO extensions of the SC scheme, vs. normalized reference stress  $\sigma_{(0)}/\tau^*$ . We observe:

- For a soft isotropic relaxation mechanism ( $\sigma_{(0)}/\tau^* < 1$ ), all extensions of the SC scheme are similar. In this case, the contribution of dislocation slip is negligible and the polycrystal behaves as an homogeneous material with no mechanical contrast between the grains.
- The TGT extension of the SC scheme shows a saturation of  $\bar{\sigma}_{(0)}/\tau^*$  at moderate values of  $\sigma_{(0)}/\tau^* \approx 20$ . It thus behaves qualitatively as the Static bound (uniform stress field), but at a higher flow stress. An important consequence is that the TGT extension allows the polycrystal to deform when  $\sigma_{(0)}/\tau^* \rightarrow \infty$  with only three independent slip systems, but this behavior is inaccurate and departs significantly from full-field computations (Castelnau et al., 2008a,b).
- For  $\sigma_{(0)}/\tau^* \gtrsim 10$ , predictions of AFF, SEC, VAR and SO formulations follow a scaling law, with  $\bar{\sigma}_{(0)}/\tau^*$  proportional to  $(\sigma_{(0)}/\tau^*)^\gamma$ . While the AFF and SEC flow stress increases rapidly leading to  $\gamma \approx 0.77$ , an overestimated growth-rate, those of the VAR and SO procedures lead to  $\gamma \approx 0.52$ . In the case where only dislocation slip was considered, this value was in perfect agreement with full-field results (Castelnau et al., 2008a,b).

Fig. 4b shows the evolution of the normalized equivalent effective strain-rate of the relaxation mechanism  $\bar{\epsilon}_{eq}^{re}/\bar{\epsilon}_{eq}$  with  $\sigma_{(0)}/\tau^*$ . Predictions of the Taylor bound show a saturation of  $\bar{\epsilon}_{eq}^{re}/\bar{\epsilon}_{eq}$  at  $\approx 0.4$ , at moderate values of  $\sigma_{(0)}/\tau^* \approx 20$ . In this approximation, the contribution of slip systems to strain cannot exceed 60%. Predictions of the AFF, SEC, VAR and SO formulations and Static bound show a scaling law for values  $\sigma_{(0)}/\tau^* \gtrsim 100$  with  $\bar{\epsilon}_{eq}^{re}/\bar{\epsilon}_{eq}$  proportional to  $(\sigma_{(0)}/\tau^*)^{-\delta}$ . The exponent  $\delta$  is larger for the Static and TGT estimates ( $\delta \approx 3.5$ , i.e. a value similar to  $n_{(0)}$ ) than for the AFF, SEC, VAR formulations

#### Linear isotropic relaxation mechanism ( $n_{(0)} = 1$ )

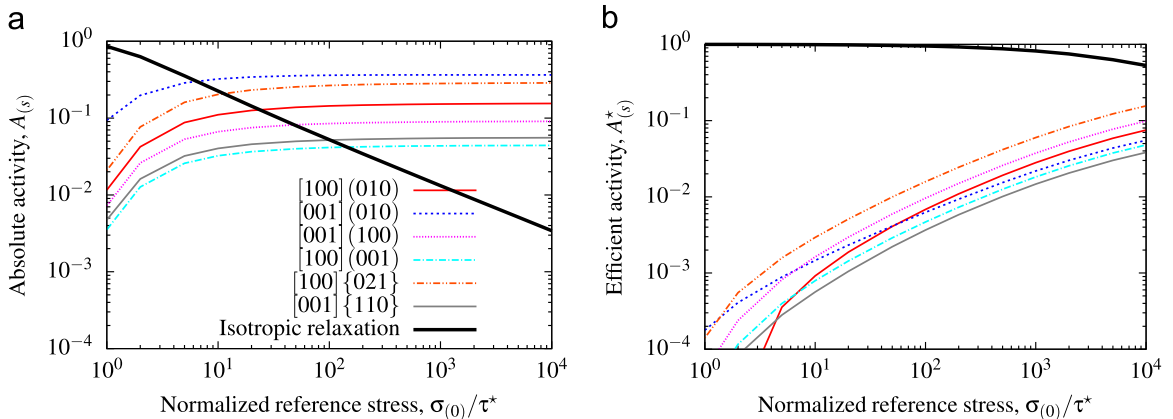
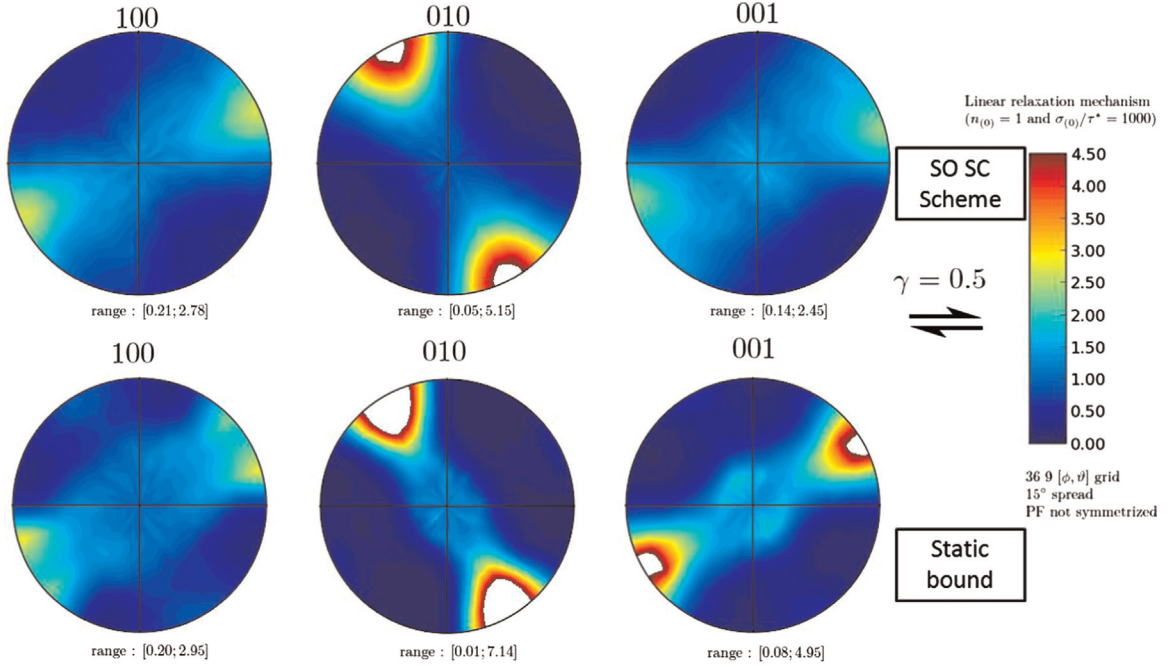


Fig. 7. Effect of the relaxation strength  $\sigma_{(0)}/\tau^*$  on the activity of all deformation mechanisms. (a) Absolute activity. (b) Efficient activity. Results from the SO extension of the SC scheme.



**Fig. 8.** Olivine pole figures obtained from the Static bound and the SO self-consistent scheme for olivine aggregate at strain  $\gamma=0.5$  and 360 km depth along a 20-Ma ocean geotherm; equal-area projection. The direction of shear is indicated.

( $\delta \approx 0.73\text{--}0.79$ ). Predictions of the SO extension lead to an intermediate value,  $\delta \approx 1.6$ .

Fig. 4(c–f) presents the evolution with  $\sigma_{(0)}/\tau^*$  of the overall normalized equivalent stress and strain-rate heterogeneities  $\Sigma(\sigma_e)/\bar{\sigma}_e$ ,  $\Sigma(\epsilon_e)/\bar{\epsilon}_e$ ,  $\Sigma(\epsilon_e^{sl})/\bar{\epsilon}_e^{sl}$  and  $\Sigma(\epsilon_e^{re})/\bar{\epsilon}_e^{re}$ , defined as

$$\Sigma(\sigma_e) = \sqrt{\langle (\sigma_e)^2 \rangle - (\bar{\sigma}_e)^2}, \quad \Sigma(\epsilon_e^{(\cdot)}) = \sqrt{\langle (\epsilon_e^{(\cdot)})^2 \rangle - (\bar{\epsilon}_e^{(\cdot)})^2} \quad (57)$$

where the superscript  $(\cdot)$  can be replaced by  $sl$  (resp.  $re$  or nothing) to define the effective strain-rate associated to all slip systems (resp. associated to relaxation mechanism or associated to both). These quantities are related to the standard deviation of stress and strain-rates in the polycrystal, combining the field fluctuations inside the grains together with the fluctuations between different grains. Note that normalized results are presented in Fig. 4c–f (and also in the forthcoming figures), with a normalized factor depending on the considered model. For example,  $\Sigma(\sigma_e)/\bar{\sigma}_e$  for the AFF model has been calculated using the AFF estimate for  $\bar{\sigma}_e$ . The discrepancies concerning the effective flow stress and effective strain-rate of relaxation mechanism, already discussed above, have thus to be taken into account to compare non-normalized values. As for  $\Sigma(\epsilon_e)/\bar{\epsilon}_e$ , since the same  $\bar{\epsilon}_e$  has been prescribed for all models, plots of  $\Sigma(\epsilon_e)/\bar{\epsilon}_e$  and  $\Sigma(\epsilon_e)$  exhibit similar shapes.

Fig. 4(c–f) shows that stress and strain-rate heterogeneities increase with the reference stress for the SEC, AFF, VAR and SO extensions of SC scheme. Again, the TGT approach exhibits a very different response, with a saturation at small  $\sigma_{(0)}/\tau^*$  values of  $\approx 5\text{--}10$ . At large  $\sigma_{(0)}/\tau^*$ , the TGT approach predicts heterogeneities  $\Sigma$  similar to those of the Taylor and Static bounds for stress and the strain-rate. By construction, the Static and Taylor bounds lead to  $\Sigma(\sigma_e) = 0$  and  $\Sigma(\epsilon_e) = 0$ , respectively.

Fig. 4f shows that strain-rate heterogeneities of the relaxation mechanism increase faster than strain-rate heterogeneities along slip systems (Fig. 4e).

It is interesting to note that for small values of  $\sigma_{(0)}/\tau^*$ , the polycrystal behavior is close to homogeneous with almost no heterogeneities of equivalent stress (Fig. 4c), equivalent strain-rate (Fig. 4d), nor equivalent strain-rates in the relaxation mechanism (Fig. 4d). Nevertheless, heterogeneities in slip system strain-rates do exist with  $\Sigma(\epsilon_e^{sl})/\bar{\epsilon}_e^{sl} \approx 1.73$  for all estimates. This is also the strain-rate heterogeneity predicted by the Static and Taylor bound, as stress and strain-rate fields both become homogeneous.

#### 4.2.2. Case $n_{(0)} = 1$ ; $n_{(k)} = 3.5$

We now consider the case in which the relaxation mechanism is linear viscous:  $n_{(0)} = 1$ . The slip systems remain non-linear with  $n_{(k)} = 3.5$ . This case is of practical interest since linear diffusion creep (e.g. Nabarro–Herring) could be an efficient relaxation mechanisms occurring in the Earth in combination with dislocation creep. Note that the TGT extension of SC scheme cannot be used here since the stress exponent  $n_{(0)}$  is different from the stress exponent for slip systems. Fig. 5

presents the influence of  $\sigma_0/\tau^*$  on the normalized effective reference stress, the normalized effective equivalent strain-rate of the relaxation mechanism, the heterogeneities of stress field, and the effective stress sensitivity  $\tilde{n}$ .

Results for the effective stress are similar to those of Fig. 4, albeit with different growth rates with  $\gamma \approx 0.5$  for the AFF and SEC estimates and  $\gamma \approx 0.4$  for the VAR and SO approximations. It can be observed that the SO estimation is the only SC extension respecting the VAR upper bound. Stress heterogeneities are for  $n_{(0)} = 1.0$  (Fig. 5c) are approximately half of those obtained for  $n_{(0)} = n_{(k)} = 3.5$  (Fig. 4c).

The contribution of relaxation mechanism to the overall strain-rate is much larger for  $n_{(0)} = 1.0$  (Fig. 5b) than for  $n_{(0)} = 3.5$  (Fig. 4b). Here,  $\delta \approx 0.6$  for VAR and SO estimates,  $\delta \approx 0.5$  for SEC and AFF approximations, and  $\delta = 1 = n_{(0)}$  for the Static bound.

The effective stress sensitivity of the polycrystal  $\tilde{n}$  (Eq. (56)) is shown in Fig. 5d. The Static bound predicts  $\tilde{n}$  ranging between  $n_{(0)}$  and  $n_{(k)}$ , depending on the activated deformation mechanisms. For the Taylor bound,  $\tilde{n}$  lies close to  $n_{(0)}$ . Other models predict  $\tilde{n}$  ranging between  $n_{(0)}$  and 2, depending on the strength of the isotropic mechanism.

Interestingly, for all but the Static bound, the value of  $\tilde{n}$  remains smaller than 2, whatever the strength of the isotropic mechanism. This result is of great practical importance: a polycrystal with less than four independent slip systems and a linear relaxation mechanism, and slip systems with a stress sensitivity of  $n_{(k)} = 3.5$  cannot exhibit an overall stress sensitivity of  $\tilde{n} \approx 3.5$ , whatever the strength of the relaxation mechanism. This observation is in contradiction with many published results for olivine, where  $\tilde{n} = n_{(k)} = 3.5$  is usually assumed or observed (Bai et al., 1991; Hirth and Kohlstedt, 2003). The additional relaxation mechanism in olivine is poorly known but, according to our calculations, it should exhibit a nonlinear behavior, i.e. it should be different from the standard diffusion creep.

#### 4.3. Influence of relaxation stress exponent $n_{(0)}$

In this section, we test the influence of the stress exponent  $n_{(0)}$  of the relaxation mechanism on the overall behavior of the aggregate. Fig. 6 presents the polycrystal properties as a function of  $n_{(0)}$ . Note that, by definition, the TGT model can only be calculated for  $n_{(0)} = 3.5$ .

Fig. 6a shows the effective stress exponent  $\tilde{n}$  for the various extensions of the SC scheme for a normalized relaxation reference stress  $\sigma_0/\tau^* = 1000$ . All curves cross at  $\tilde{n} = n_{(k)} = n_{(0)} = 3.5$ , when all mechanisms share the same stress exponent. For the Static bounds,  $\tilde{n}$  shows no dependence with  $n_{(0)}$  since the easiest mechanism controls the effective behavior. At the opposite,  $\tilde{n}$  is equal to the exponent of the toughest mechanism  $n_{(0)}$  for the Taylor bounds. The AFF and SEC models (superimposed in the figure) also predict an overall stress sensitivity essentially proportional to  $n_{(0)}$ , with a slope  $\approx 0.8$ . On the other hand, the VAR and SO extensions of SC scheme feature similar non-linear evolutions of  $\tilde{n}$  with  $n_{(0)}$ . For  $n_{(0)} < 3.5$ ,  $\tilde{n}$  is found larger than that predicted by AFF and SEC models, whereas the opposite is observed for  $n_{(0)} > 3.5$ .

Fig. 6b shows the normalized equivalent effective strain-rate of the relaxation mechanism  $\bar{\epsilon}_{eq}^{re}/\bar{\epsilon}_{eq}$ . The AFF, SEC and VAR models predict relatively large values ranging between  $10^{-1}$  and  $10^{-3}$ . The SO model predicts a much lower contribution of the relaxation mechanism, lower than  $10^{-8}$  for  $n_{(0)} = 10$ . For comparison, for Taylor bound,  $\sim 40\%$  of the strain is produced by the isotropic relaxation mechanism, whatever the value of  $n_{(0)}$ .

Fig. 6c shows the normalized effective reference stress  $\bar{\sigma}_0/\tau^*$ . The VAR and SO extensions are similarly weakly dependent on  $n_{(0)}$ . As above, only the SO estimate respects the VAR upper bound, AFF and SEC estimates providing an effective stress 5–10 times larger.

Fig. 6(d–f) presents the overall normalized stress and strain-rate heterogeneities  $\Sigma(\sigma_e)/\bar{\sigma}_e$ ,  $\Sigma(\epsilon_e^{sl})/\bar{\epsilon}_e^{sl}$  and  $\Sigma(\epsilon_e^{re})/\bar{\epsilon}_e^{re}$ . For the Static and Taylor bounds, heterogeneities are small and independent of  $n_{(0)}$ . For the SC extensions, and in particular the SO model, heterogeneities increase with  $n_{(0)}$ , and can be quite large, resulting in significant stress and strain heterogeneities in the aggregate. In this case, activation of deformation mechanisms might be very localized in the material, probably next to grain boundaries where field heterogeneities are generally larger than in grain interior. Such an observation could be used as a guide for future experimental work.

#### 4.4. Mechanism activities

Two kinds of activity are defined to compare the contribution of the different types of deformation mechanism (dislocation slip and relaxation) to the overall polycrystal deformation. We define on one hand the phase average strain-rate tensor  $\bar{\underline{\epsilon}}_{(s)}^{(r)}$  for the slip family ( $s$ ) and the associated equivalent strain-rate  $\bar{\epsilon}_{(s)eq}^{(r)}$

$$\bar{\underline{\epsilon}}_{(s)}^{(r)} = \sum_{k \in s} \langle \dot{\gamma}_{(k)} \rangle^{(r)} \underline{\mu}_{(k)}^{(r)} \quad (\text{for } s > 0) \quad \text{and} \quad \bar{\epsilon}_{(s)eq}^{(r)} = \sqrt{\frac{2}{3} \bar{\underline{\epsilon}}_{(s)}^{(r)} : \bar{\underline{\epsilon}}_{(s)}^{(r)}}. \quad (58)$$

and on the other hand the equivalent strain-rate of the relaxation mechanism

$$\bar{\epsilon}_{(0)eq}^{(r)} = \sqrt{\frac{2}{3} \bar{\underline{\epsilon}}_{(0)}^{(r)} : \bar{\underline{\epsilon}}_{(0)}^{(r)}}. \quad (59)$$

The first activity, called here the ‘absolute activity’ and denoted  $A_{(s)}$ , represents the global equivalent strain-rate produced by each deformation mechanism (slip system family for  $s \geq 1$ , and isotropic relaxation mechanism for  $s=0$ ):

$$A_{(s)} = \frac{1}{A^0} \sum_{r=1}^N c^{(r)} \bar{\epsilon}_{(s)}^{(r)}{}_{eq}, \quad \text{where } A^0 = \sum_{s=0}^S A_{(s)}. \quad (60)$$

The second activity is the projection on the macroscopic response of the strain-rate due to the deformation mechanism ( $s$ ); it is called the 'efficient activity', denoted  $A_{(s)}^*$ , and defined as

$$A_{(s)}^* = \sum_{r=1}^N c^{(r)} \frac{\bar{\epsilon}_{(s)}^{(r)} : \bar{\epsilon}}{\bar{\epsilon} : \bar{\epsilon}}, \quad s \in [0, S]. \quad (61)$$

Note that both activities are normalized, i.e.  $\sum_{s=0}^S A_{(s)} = \sum_{s=0}^S A_{(s)}^* = 1$ . We have defined these two activities in order to address the effect of local strain heterogeneities (absolute activity) and the impact of a mechanism on the macroscopic deformation (efficient activity). For example, if a given mechanism generates opposite strains in two phases, the absolute activity will be large and the efficient activity will vanish.

Fig. 7a shows the evolution of the absolute activities with  $\sigma_{(0)}/\tau^*$ . First of all, the absolute activity of the relaxation mechanism decreases quickly with  $\sigma_{(0)}/\tau^*$ ; it is less than 5% for  $\sigma_{(0)}/\tau^* > 100$  and 2% for  $\sigma_{(0)}/\tau^* > 1000$ . At relatively small value of  $\sigma_{(0)}/\tau^* \approx 10$ , the absolute activity of the easiest system [001](010) becomes larger than that of the isotropic mechanism. An unexpected result of the simulation is the high absolute activity of [100]{021} slip family, despite its high CRSS. This is due to the heterogeneity of the stress field.

Fig. 7b shows the evolution of the efficient activities with  $\sigma_{(0)}/\tau^*$ . The efficient activity of the relaxation mechanism remains dominant for the whole range. The efficient activities of slip systems remain smaller than 10%. Despite its low CRSS and large absolute activity, the efficient activity of [001](010) slip is relatively small. Indeed, efficient activities are not correlated with the CRSS. Finally, at relatively large  $\sigma_{(0)}/\tau^*$ , the absolute activity of the isotropic relaxation mechanism is weak although its efficient activity remains dominant.

#### 4.5. Crystallographic texture evolution

Fig. 8 shows the LPO predicted by the SO extension of SC scheme and Static bound estimates with linear relaxation mechanism ( $n_{(0)} = 1$ ,  $\sigma_{(0)}/\tau^* = 1000$ ) for simple shear corresponding to an equivalent strain of 0.5. Here, the static bound is used for comparison as this rather intuitive model is often used in the geophysical community, for example to infer the in situ deformation history of a specimen that might explain the observed texture. The Static bound which favors the easiest deformation mechanism leads to align the olivine [001] axis with the shear direction and the (010) plane with the shear plane strain, due to the large activation of the easiest system [001](010). The obtained pole figures are close to the so-called *C-Type* texture according the classification of Jung and Karato (2001). The texture obtained with the SO extension is less marked, with a much weaker alignment of the [100] axes with the shear direction. This texture corresponds to a mixed *Type-A* and *C-Type* texture of Jung and Karato (2001). This sensitivity of texture evolution to the used micromechanical model results from the complex stress and strain-rate heterogeneities discussed above.

## 5. Conclusion

Our study introduces a novel treatment of the effective viscoplastic behavior in polycrystals lacking four independent slip systems, in which a relaxation mechanism is accounted for. The method is implemented into several nonlinear extensions of the SC scheme, including the SEC, AFF, TGT, VAR and SO order estimates. Two extensions of the SO estimate introduced by Liu et al. (2003b) have been proposed: the first is based on the use of a tensorial basis to linearize the isotropic relaxation mechanism as in Idiart et al. (2006); the second is based on an approximation of the potential of the relaxation mechanism. The main limitation of the first strategy is that results depend on the choice of the tensor basis; the criteria for isotropic and numerical convergence cannot be met simultaneously. Although the second strategy introduces a new approximation, it satisfies the isotropy criterion while ensuring the convergence of the attractive fixed-point algorithm.

The case of olivine, a mineral phase of geophysical interest, is presented as an illustrative example. The main results can be summarized as follows:

- The SO extension of the SC scheme predicts a very large strain-rate heterogeneity of the relaxation mechanism.
- All non-linear extensions of the SC scheme predict that when using a linear viscous relaxation process, the effective stress sensitivity of the polycrystal is significantly smaller than those of the slip systems (set to  $n_{(k)}=3.5$ ).
- The relaxation mechanism significantly influences the effective reference stress of the polycrystal even if its absolute activity is very small.
- The SO extension predicts that for  $\sigma_0/\tau^* > 100$ , the isotropic relaxation mechanism is very efficient to accommodate the macroscopic strain although it is less active than all other dislocation slip systems.
- The SO extension of SC scheme predicts different textures than those provided by the static bound.

For geophysical applications, our study highlights the strong effects of the intergranular mechanical interactions arising inside a polycrystal. Capturing correctly these interactions, as done with the SO extension of SC scheme, is a prerequisite condition for making correct connections between processes at the slip system level and the overall polycrystal response. In agreement with previous studies (Liu et al., 2003a,b; Lebensohn et al., 2007), this leads to an improved description of LPO development compared to those provided by classical TGT SC and Static bound estimates (Wenk et al., 1991; Tommasi et al., 1999, 2000; Blackman et al., 2002; Chastel et al., 1993; Dawson and Wenk, 2000).

Here, we replace the fictitious  $\langle 1\bar{1}0 \rangle \{111\}$  slip system used in previous studies by a more realistic isotropic relaxation mechanism. It can be noticed that, when using the SO SC scheme, the present results are qualitatively similar to those obtained previously in Castelnau et al. (2006, 2008a,b, 2009, 2010) with  $\langle 1\bar{1}0 \rangle \{111\}$  slips. In the future the present model will be improved by implementing other mechanisms such as dislocation climb (Lebensohn et al., 2010) or disclinations (Cordier et al., 2014) with a refined input from experimental data. This model could also be applied to other important crystalline phases present in the Earth mantle such as diopsides and garnets, as well as multiphase materials (e.g. Raterron et al., 2014).

## Acknowledgments

This research was supported by the Centre National de la Recherche Scientifique CNRS, as well as the Agence Nationale de la Recherche (ANR) Grant BLAN08-2\_343541 ‘‘Mantle Rheology’’.

## Appendix A. Expressions of linearized compliance tensor

$$\underline{\underline{M}}_{SEC}^{(r)} = \frac{3}{2} \frac{\partial_{\sigma_e} \phi_{(0)}^{(r)}(\bar{\sigma}_e^{(r)})}{\bar{\sigma}_e^{(r)}} \underline{\underline{K}} + \sum_{k=1}^K \frac{\partial_{\tau} \phi_{(k)}^{(r)}(\bar{\tau}_{(k)}^{(r)})}{\bar{\tau}_{(k)}^{(r)}} \underline{\underline{\mu}}_{(k)}^{(r)} \otimes \underline{\underline{\mu}}_{(k)}^{(r)} \quad (\text{A.1})$$

$$\begin{aligned} \underline{\underline{M}}_{AFF}^{(r)} &= \frac{3}{2} \frac{\partial_{\sigma_e} \phi_{(0)}^{(r)}(\bar{\sigma}_e^{(r)})}{\bar{\sigma}_e^{(r)}} \underline{\underline{K}} + \left( \partial_{\sigma_e \sigma_e}^2 \phi_{(0)}^{(r)}(\bar{\sigma}_e^{(r)}) - \frac{\partial_{\sigma_e} \phi_{(0)}^{(r)}(\bar{\sigma}_e^{(r)})}{\bar{\sigma}_e^{(r)}} \right) \underline{\underline{n}}^{(r)} \otimes \underline{\underline{n}}^{(r)} \\ &+ \sum_{k=1}^K \frac{\partial_{\tau \tau}^2 \phi_{(k)}^{(r)}(\bar{\tau}_{(k)}^{(r)})}{\bar{\tau}_{(k)}^{(r)}} \underline{\underline{\mu}}_{(k)}^{(r)} \otimes \underline{\underline{\mu}}_{(k)}^{(r)} \end{aligned} \quad (\text{A.2})$$

$$\underline{\underline{M}}_{VAR}^{(r)} = \frac{3}{4} \frac{\partial_{\sigma_e} \phi_{(0)}^{(r)}(\sqrt{\langle \sigma_e^2 \rangle^{(r)}})}{\sqrt{\langle \sigma_e^2 \rangle^{(r)}}} \underline{\underline{K}} + \sum_{k=1}^K \frac{1}{2} \frac{\partial_{\tau} \phi_{(k)}^{(r)}(\sqrt{\langle \tau_{(k)}^2 \rangle^{(r)}})}{\sqrt{\langle \tau_{(k)}^2 \rangle^{(r)}}} \underline{\underline{\mu}}_{(k)}^{(r)} \otimes \underline{\underline{\mu}}_{(k)}^{(r)} \quad (\text{A.3})$$

where  $\underline{\underline{n}}^{(r)} = \frac{3}{2} \bar{\sigma}'^{(r)} / \bar{\sigma}_e^{(r)}$  and

$$\langle \sigma_e^2 \rangle^{(r)} = \frac{3}{2} \underline{\underline{K}} :: \langle \underline{\underline{\sigma}} \otimes \underline{\underline{\sigma}} \rangle^{(r)}, \quad \langle \tau_{(k)}^2 \rangle^{(r)} = \underline{\underline{\mu}}_{(k)}^{(r)} \otimes \underline{\underline{\mu}}_{(k)}^{(r)} :: \langle \underline{\underline{\sigma}} \otimes \underline{\underline{\sigma}} \rangle^{(r)} \quad (\text{A.4})$$

Here  $\underline{\underline{K}}$  is the third order deviatoric projection tensor, such as  $\underline{\underline{\sigma}}' = \underline{\underline{K}} : \underline{\underline{\sigma}}$ .

## Appendix B. Lequeu tensor basis

Lequeu et al. (1987) have defined the following orthonormal basis for symmetric deviatoric tensor

$$\begin{aligned} \underline{\underline{\alpha}}_1 &= \frac{\sqrt{2}}{2} (\underline{\underline{e}}_2 \otimes \underline{\underline{e}}_2 - \underline{\underline{e}}_1 \otimes \underline{\underline{e}}_1), & \underline{\underline{\alpha}}_2 &= \frac{\sqrt{6}}{6} (2\underline{\underline{e}}_3 \otimes \underline{\underline{e}}_3 - \underline{\underline{e}}_1 \otimes \underline{\underline{e}}_1 - \underline{\underline{e}}_2 \otimes \underline{\underline{e}}_2), \\ \underline{\underline{\alpha}}_3 &= \frac{\sqrt{2}}{2} (\underline{\underline{e}}_2 \otimes \underline{\underline{e}}_3 + \underline{\underline{e}}_3 \otimes \underline{\underline{e}}_2), & \underline{\underline{\alpha}}_4 &= \frac{\sqrt{2}}{2} (\underline{\underline{e}}_3 \otimes \underline{\underline{e}}_1 + \underline{\underline{e}}_1 \otimes \underline{\underline{e}}_3), \\ \underline{\underline{\alpha}}_5 &= \frac{\sqrt{2}}{2} (\underline{\underline{e}}_1 \otimes \underline{\underline{e}}_2 + \underline{\underline{e}}_2 \otimes \underline{\underline{e}}_1). \end{aligned}$$

## References

- Argon, A., 1997. Morphological mechanisms and kinetics of large-strain plastic deformation and evolution of texture in semicrystalline polymers. *J. Comput. Aided Mater.* 4, 75–98.
- Bai, Q., Mackwell, S.J., Kohlstedt, D.L., 1991. High-temperature creep of olivine single crystals; 1. Mechanical results for buffered samples. *J. Geophys. Res.* 96, 2441–2463.
- Bazant, Z.P., Oh, B.H., 1986. Efficient numerical integration on the surface of sphere. *Z. Angew. Math. U. Mech.* 66, 37–49.

- Bhattacharya, A., El-Danaf, E., Kalidindi, S.R., Doherty, R.D., 2001. Evolution of grain-scale microstructure during large strain simple compression of polycrystalline aluminium with quasi-columnar grains: OIM measurements and numerical simulations. *Int. J. Plast.* 17, 861–883.
- Blackman, D.K., Wenk, H.R., Kendall, J.M., 2002. Seismic anisotropy of the upper mantle: 1. Factors that affect mineral texture and effective elastic properties. *Geochem. Geophys. Geosyst.* 3, 8601.
- Bobeth, M., Diener, G., 1987. Static and thermoelastic field fluctuations in multiphase composites. *J. Mech. Phys. Solids* 35, 137–149.
- Bornert, M., Masson, R., Ponte Castañeda, P., Zaoui, A., 2001. Second-order estimates for the effective behaviour of viscoplastic polycrystalline materials. *J. Mech. Phys. Solids* 49, 2737–2764.
- Bornert, M., Ponte Castañeda, P., 1998. Second-order estimates of the self-consistent type for viscoplastic polycrystals. *Proc. R. Soc. Ser. A and Ser. B A454*, 3035–3045.
- Bowden, P., Young, R., 1974. Deformation mechanisms in crystalline polymers. *J. Mater. Sci.* 9, 2034–2051.
- Brenner, R., Castelnau, O., Badea, L., 2004. Mechanical field fluctuations in polycrystals estimated by homogenization techniques. *Proc. R. Soc. Ser. A and Ser. B A460 (2052)*, 3589–3612.
- Castelnau, O., Blackman, D.K., Becker, T.W., 2009. Numerical simulations of texture development and associated rheological anisotropy in regions of complex mantle flow. *Geophys. Res. Lett.* 36 (L12304).
- Castelnau, O., Blackman, D.K., Lebensohn, R.A., Ponte Castañeda, P., 2008a. Micromechanical modelling of the viscoplastic behavior of olivine. *J. Geophys. Res.* 113.
- Castelnau, O., Brenner, R., Lebensohn, R., 2006. The effect of strain heterogeneity on the work-hardening of polycrystals predicted by mean-field approaches. *Acta Mater.* 54, 2745–2756.
- Castelnau, O., Cordier, P., Lebensohn, R.A., Merkel, S., Raterron, P., 2010. Microstructures and rheology of the earth's upper mantle inferred from multiscale approach. *C. R. Méc.* 11, 304–315.
- Castelnau, O., Lebensohn, R.A., Ponte Castañeda, P., Blackman, D.K., 2008b. Earth mantle rheology inferred from homogenization theories. In: *Multi-scale Modeling of Heterogeneous Materials*. John Wiley and Sons, Hoboken, pp. 55–70.
- Chastel, Y., Dawson, P.R., Wenk, H.-R., Bennett, K., 1993. Anisotropic convection with implications for the upper mantle. *J. Geophys. Res.* 98 (B10), 757–771.
- Cordier, P., Demouchy, S., Beausir, B., Taupin, V., Barou, F., Fressengeas, C., 2014. Disclinations provide the missing mechanism for deforming olivine-rich rocks in the mantle. *Nature* 507, 51–56.
- Dawson, P.R., Wenk, H.-R., 2000. Texturing of the upper mantle convection. *Philos. Mag.* A 80, 573–598.
- de Botton, G., Ponte Castañeda, P., 1995. Variational estimates for the creep behaviour of polycrystals. *Proc. R. Soc. Ser. A and Ser. B A448*, 121–142.
- Eshelby, J.D., 1957. The determination of the elastic field of an ellipsoidal inclusion, and related problems. *Proc. R. Soc. Ser. A and Ser. B A241*, 376–396.
- Gilormini, P., 1995. A critical evaluation for various nonlinear extensions of the self-consistent model. In: Pineau, A., Zaoui, A. (Eds.), *IUTAM Symposium on Micromechanics of Plasticity and Damage of Multiphase Materials (Severe, France)*. Kluwer Academic Publishers, pp. 67–74.
- Hill, R., 1965. Continuum micro-mechanics of elastoplastic polycrystals. *J. Mech. Phys. Solids* 13, 89.
- Hirth, G., Kohlstedt, D.L., 2003. Rheology of the upper mantle and the mantle wedge: a view from the experimentalists. In: *Inside the Subduction Factory*. Geophysical Monograph Series, vol. 138, pp. 83–105.
- Hutchinson, J.W., 1976. Bounds and self-consistent estimates for creep of polycrystalline materials. *Proc. R. Soc. Lond. A* 348, 101–127.
- Hutchinson, J.W., 1977. Creep and plasticity of hexagonal polycrystals related to single crystal slip. *Metall. Trans. A and B* 8A, 1465–1469.
- Idiart, M.I., Moulinc, H., Ponte Castañeda, P., Suquet, P., 2006. Macroscopic behavior and field fluctuations in viscoplastic composites: second-order estimates versus full-field simulations. *J. Mech. Phys. Solids* 54, 1029–1063.
- Idiart, M.I., Ponte Castañeda, P., 2005. Second-order estimates for nonlinear isotropic composites with spherical pores and rigid particles. *C. R. Méc.* 333, 147–154.
- Idiart, M.I., Ponte Castañeda, P., 2007. Variational linear comparison bounds for nonlinear composites with anisotropic phases. ii. Crystalline materials. *Proc. R. Soc. A* 463, 925–943.
- Jung, H., Karato, S., 2001. Water-induced fabric transitions in olivine. *Science* 293, 1460–1463.
- Kaminski, E., Ribe, N.M., 2001. A kinematic model for recrystallization and texture development in olivine polycrystal. *Earth Planet. Sci. Lett.* 189, 744–752.
- Kanit, T., Forest, S., Galliet, I., Mounoury, V., Jeulin, D., 2003. Determination of the size of the representative volume element for random composites: statistical and numerical approach. *Int. J. Solids Struct.* 40, 3647–3679.
- Karato, S.I., 2007. Comments on “petrofabrics and seismic properties of garnet peridotites from the usp Sulu terrane (China)” by Xu et al. [*Tectonophysics* 421 (2006) 111–127]. *Tectonophysics* 429, 287–289.
- Kreher, W., 1990. Residual stresses and stored elastic energy of composites and polycrystals. *J. Mech. Phys. Solids* 38, 115–128.
- Laws, N., 1973. On the thermodynamics of composite materials. *J. Mech. Phys. Solids* 21, 9–17.
- Lebensohn, R.A., 2001. N-site modeling of a 3-d viscoplastic polycrystal using fast fourier transform. *Acta Mater.* 49, 2723–2737.
- Lebensohn, R.A., Hartley, C.S., Tomé, C.N., Castelnau, O., 2010. Modelling the mechanical response of polycrystals deforming by climb and glide. *Philos. Mag.* 90 (5), 567–583.
- Lebensohn, R.A., Ponte Castañeda, P., Brenner, R., Castelnau, O., 2011. Full-field vs. homogenization methods to predict microstructure-property relations for polycrystalline materials. In: *Computational Methods for Microstructure-Property Relationships*. Springer, New York, pp. 393–441.
- Lebensohn, R.A., Tomé, C.N., 1993. A selfconsistent approach for the simulation of plastic deformation and texture development of polycrystals: application to zirconium alloys. *Acta. Metall. Mater.* 41, 2611–2624.
- Lebensohn, R.A., Tomé, C.N., Ponte Castañeda, P., 2007. Self-consistent modeling of the mechanical behavior of viscoplastic polycrystals incorporating field fluctuations. *Philos. Mag. A and B* 87 (28), 4287–4322.
- Lequeu, Y., Gilormini, P., Montheillet, F., Bacroix, B., Jonas, J.J., 1987. Yield surfaces for textured polycrystals. 1. Crystallographic approach. *Acta Metall.* 35, 439–451.
- Liu, Y., Gilormini, P., Ponte Castañeda, P., 2003a. Homogenization estimates for texture evolution in halite. *Tectonophysics* 406, 179–195.
- Liu, Y., Gilormini, P., Ponte Castañeda, P., 2003b. Variational self-consistent estimates for texture evolution in viscoplastic polycrystals. *Acta Mater.* 51, 5425–5437.
- Liu, Y., Ponte Castañeda, P., 2004. Second-order theory for the effective behavior and field fluctuations in viscoplastic polycrystals. *J. Mech. Phys. Solids* 52, 467–495.
- Masson, R., Bornert, M., Suquet, P., Zaoui, A., 2000. Affine formulation for the prediction of the effective properties of nonlinear composites and polycrystals. *J. Mech. Phys. Solids* 48, 1203–1227.
- Molinari, A., Canova, G.R., Ahzi, S., 1987. Self consistent approach of the large deformation polycrystal viscoplasticity. *Acta Metall.* 35, 2983–2994.
- Moulinec, H., Suquet, P., 1998. A numerical method for computing the overall response of nonlinear composites with complex microstructure. *Comput. Methods Appl. Mech. Eng.* 157, 69–94.
- Nebozhyn, M.V., Gilormini, P., Ponte Castañeda, P., 2000. Variational self-consistent estimates for viscoplastic polycrystals with highly anisotropic grains. *C. R. Acad. Sci. Paris* 318 (IIB), 11–17.
- Parks, D.M., Ahzi, S., 1990. Polycrystalline plastic deformation for crystals lacking five independent slip systems. *J. Mech. Phys. Solids* 38, 701–724.
- Ponte Castañeda, P., 1991. The effective mechanical properties of nonlinear isotropic composites. *J. Mech. Phys. Solids* 39, 45–71.
- Ponte Castañeda, P., 1996. Exact second-order estimates for the effective mechanical properties of nonlinear composites. *J. Mech. Phys. Solids* 44, 827–862.
- Ponte Castañeda, P., 2002. Second-order homogenization estimates for nonlinear composites incorporating field fluctuations. 1—theory. *J. Mech. Phys. Solids* 50, 737–757.
- Ponte Castañeda, P., Suquet, P., 1998. Nonlinear composites. *Adv. Appl. Mech.* 34, 171–302.
- Raterron, P., Detrez, F., Castelnau, O., Bollinger, C., Cordier, P., Merkel, S., 2014. Multiscale modeling of upper mantle plasticity: from single-crystal rheology to multiphase aggregate deformation. *Phys. Earth Planet. Int.* 228, 232–243.
- Ribe, N.M., Yu, Y., 1991. A theory for plastic deformation and textural evolution for olivine polycrystals. *J. Geophys. Res.* B5, 8325–8335.
- Sarma, G.B., Dawson, P.R., 1996. Effects of interactions among crystals on the inhomogeneous deformation of polycrystals. *Acta Mater.* 44, 1937–1953.
- Seguela, R., 2007. Plasticity of semi-crystalline polymers: crystal slip versus melting-recrystallization. *e-Polymers* 7, 382–401, <http://dx.doi.org/10.1515/epoly.2007.71.382>.

- Suquet, P., 1995. Overall properties of nonlinear composites: a modified secant moduli theory and its link with Ponte Castañeda nonlinear variational procedure. *C. R. Acad. Sci. Paris* 320 (IIb), 563–571.
- Tommasi, A., Mainprice, D., Canova, G., Chastel, Y., 2000. Viscoplastic self-consistent and equilibrium-based modeling of olivine lattice preferred orientations: implications for the upper mantle seismic anisotropy. *J. Geophys. Res.* 105, 7893–7908.
- Tommasi, A., Tikoff, B., Vauchez, A., 1999. Upper mantle tectonics: three-dimensional deformation, olivine crystallographic fabrics and seismic properties. *Earth Planet. Sci. Lett.* 168, 173–186.
- Wenk, H.-R., Bennett, K., Canova, G.R., Molinari, A., 1991. Modelling plastic deformation of peridotite with self-consistent theory. *J. Geophys. Res.* 96, 8337–8349.
- Willis, J.R., 1977. Bounds and self-consistent estimates for the overall moduli of anisotropic composites. *J. Mech. Phys. Solids* 25, 185–202.
- Willis, J.R., 1981. Variational and related methods for the overall properties of composites. *Adv. Appl. Mech.* 21, 1–78.